A comparative study of the cryo-EM structures of *S. cerevisiae* and human anaphase-promoting complex/cyclosome (APC/C)

Ester Vazquez-Fernandez[1], Jing Yang[1], Ziguo Zhang[1], Antonina E. Andreeva[1], Paul Emsley[1] and David Barford[1,2]

[1]MRC Laboratory of Molecular Biology, Cambridge, CB2 0QH, UK.

[2]Corresponding author. email: dbarford@mrc-lmb.cam.ac.uk

Abstract

The anaphase-promoting complex/cyclosome (APC/C) is a large multi-subunit E3 ubiquitin ligase that controls progression through the cell cycle by orchestrating the timely proteolysis of mitotic cyclins and other cell cycle regulatory proteins. Although structures of multiple human APC/C complexes have been extensively studied over the past decade, the *S. cerevisiae* APC/C has been less extensively investigated. Here, we describe medium resolution structures of three *S. cerevisiae* APC/C complexes: unphosphorylated apo-APC/C and the ternary APC/C^{CDH1}-substrate complex, and phosphorylated apo-APC/C. Whereas the overall architectures of human and *S. cerevisiae* APC/C are conserved, as well as the mechanism of CDH1 inhibition by CDK-phosphorylation, specific variations exist, including striking differences in the mechanism of coactivator-mediated stimulation of E2 binding, and the activation of APC/C^{CDC20} by phosphorylation. In contrast to human APC/C in which coactivator induces a conformational change of the catalytic module APC2:APC11 to allow E2 binding, in *S. cerevisiae* apo-APC/C the catalytic module is already positioned to bind E2. Furthermore, we find no evidence of a phospho-regulatable auto-inhibitory segment of APC1, that in the unphosphorylated human APC/C, sterically blocks the CDC20$^{C\text{-}box}$ binding site of APC8. Thus, although the functions of APC/C are conserved from *S. cerevisiae* to humans, molecular details relating to their regulatory mechanisms differ.

Introduction

The anaphase-promoting complex/cyclosome (APC/C), through targeting specific proteins for proteolysis via the ubiquitin-proteosome system, is a key regulator of cell cycle transitions. APC/C activity and substrate selection are controlled at various levels to ensure that specific cell cycle events occur in the correct order and time, reviewed in (Alfieri, Zhang et al. 2017, Watson, Brown et al. 2019, Barford 2020, Bodrug, Welsh et al. 2021). These regulatory mechanisms include the binding of cell cycle-specific coactivator subunits (CDC20 and CDH1), reversible APC/C and coactivator phosphorylation, and inhibitory complexes and proteins.

Research on *S. cerevisiae* APC/C over 25 years provided insights into APC/C structure and mechanism. Analysis of the sequences of proteins encoded by the CDC16, CDC23 and CDC27 genes led to the characterisation of the 34-residue tetratricopeptide repeat (TPR) motif that is usually arranged in multiple copies in contiguous arrays (Sikorski, Michaud et al. 1991, Lamb, Michaud et al. 1994, King, Peters et al. 1995). Similar arrangements of TPR motifs, that serve as protein-protein interaction sites, are conserved across a range of proteins with widely varying functions. The isolation of endogenous APC/C from *S. cerevisiae* confirmed the composition of large APC/C subunits that form a MDa-sized complex, and also the discovery of four small subunits (APC9, APC12/CDC26, APC13/SWM1 and APC15/MND2) (Zachariae, Shin et al. 1996, Zachariae, Shevchenko et al. 1998, Hall, Torres et al. 2003, Passmore, McCormack et al. 2003), that are also conserved with metazoan APC/C. *S. cerevisiae* APC/C was one of the first large multi-subunit complexes to be reconstituted *in vitro* using the baculovirus/insect cell over-expression system (Schreiber, Stengel et al. 2011). Early

electron microscopy studies of endogenous and recombinant *S. cerevisiae* APC/C revealed that a TPR module and a platform module assemble to create a triangular-shaped complex defining a central cavity which accommodates a combined substrate recognition module of the coactivator and APC10, and the catalytic module of APC2:APC11 (Ohi, Feoktistova et al. 2007, da Fonseca, Kong et al. 2011, Schreiber, Stengel et al. 2011). Coactivator and APC10 cooperate to generate a co-receptor for D-box degron recognition (Carroll and Morgan 2002, Carroll, Enquist-Newman et al. 2005, Buschhorn, Petzold et al. 2011, da Fonseca, Kong et al. 2011, Chao, Kulkarni et al. 2012, Chang, Zhang et al. 2014, Brown, VanderLinden et al. 2015, Hartooni, Sung et al. 2022), whereas coactivator alone binds the KEN box and ABBA motif degrons (Chao, Kulkarni et al. 2012, Tian, Li et al. 2012, He, Chao et al. 2013).

Two coactivator subunits CDH1 and CDC20 determine APC/C substrate specificity throughout the mitotic cell cycle. The switching of these two coactivators regulates changes in APC/C substrate specificity. Additionally, coactivator-independent factors contribute to changes in substrate specificity (Lu, Hsiao et al. 2014). CDH1 interacts with the APC/C during G1, whereas CDH1 phosphorylation at the onset of S-phase inhibits its binding to the APC/C, a process that determines the irreversible transition from G1 into S-phase. On entering mitosis, CDK and polo kinases phosphorylate the APC/C to stimulate CDC20 binding to the APC/C (Lahav-Baratz, Sudakin et al. 1995, Zachariae, Schwab et al. 1998, Shteinberg, Protopopov et al. 1999, Kramer, Scheuringer et al. 2000, Rudner and Murray 2000, Golan, Yudkovsky et al. 2002, Kraft, Vodermaier et al. 2005). In contrast to metazoan APC/C, *S. cerevisiae* APC/C utilises a third coactivator (Ama1) to regulate the events of meiosis (Cooper, Mallory et al. 2000). As for human APC/C, *S. cerevisiae* APC/C functions using two E2s, a priming E2 that directly ubiquitylates APC/C substrates (Ubc4), and a processive E2 (Ubc1) that extends these ubiquitin moieties (Rodrigo-Brenni, Foster et al. 2010). Whereas the processive E2 that pairs with human APC/C (UBE2S) extends ubiquitin chains through K11 linkages (Jin, Williamson et al. 2008, Garnett, Mansfeld et al. 2009, Williamson, Wickliffe et al. 2009, Matsumoto, Wickliffe et al. 2010, Wickliffe, Lorenz et al. 2011), Ubc1 of *S. cerevisiae* synthesises K48-linked chains (Rodrigo-Brenni, Foster et al. 2010). Ubc4 and Ubc1 both bind the RING domain of APC11, and therefore compete for APC/C binding (Rodrigo-Brenni and Morgan 2007, Girard, Tenthorey et al. 2015). Ubc1 possesses an accessory UBA that enhances its affinity for the APC/C (Girard, Tenthorey et al. 2015). The activities of both *S. cerevisiae* and human APC/C are inhibited by the mitotic checkpoint complex (MCC) (Sudakin, Chan et al. 2001, Burton and Solomon 2007), whereas Acm1 (Martinez, Jeong et al. 2006) and EMI1 (early mitotic inhibitor 1) (Reimann, Freed et al. 2001, Reimann, Gardner et al. 2001, Cappell, Mark et al. 2018) are specific to *S. cerevisiae* and metazoan APC/C, respectively. These inhibitors exert their effects through a combination of pseudo-substrate motifs that block degron-binding sites on APC/C:coactivator complexes, and inhibition of E3 ligase catalytic activity by occluding E2 binding.

For our earlier research on the structure and mechanism of the APC/C we investigated the *S. cerevisiae* system due to the ease of purifying TAP-tagged APC/C from yeast cultures (Passmore, McCormack et al. 2003, Passmore, Barford et al. 2005), and at the time the benefits of yeast genetics had provided considerable insights into its function. By 2011 our capacity to over-express recombinant APC/C using the baculovirus insect cell system (Schreiber, Stengel et al. 2011, Zhang, Yang et al. 2013, Zhang, Yang et al. 2016) allowed us and others to investigate human APC/C. These studies, together with those of others, provided insights into the overall architecture of the APC/C, mechanisms of substrate recognition and ubiquitylation, and APC/C regulation through mechanisms including reversible phosphorylation and the binding of the mitotic checkpoint complex and EMI1 (Frye, Brown et al. 2013, Brown, Watson et al. 2014, Chang, Zhang et al. 2014, Brown, VanderLinden et al. 2015, Chang, Zhang et al. 2015, Alfieri, Chang et al. 2016, Brown, VanderLinden et al. 2016, Yamaguchi, VanderLinden et al. 2016, Zhang, Chang et al. 2016, Watson, Grace et al. 2019, Höfler, Yu et al. 2024).

Recently, we returned to *S. cerevisiae* APC/C to extend the 10 Å-resolution structure published in 2011 (da Fonseca, Kong et al. 2011, Schreiber, Stengel et al. 2011) to atomic resolution. We completed building a 4.0 Å structure of the *S. cerevisiae* APC/C^{CDH1}-substrate complex (APC/C$^{CDH1:Hsl1}$), allowing a comparative study of the *S. cerevisiae* and human systems. While human and *S. cerevisiae* APC/C architectures are in general very similar, there are significant differences, including the additional TPR subunit APC7 in human APC/C, and the structures of the smaller, less well conserved subunits. Aspects of regulation also differ. For example, in contrast to human APC/C, the catalytic module APC2:APC11 of *S. cerevisiae* adopts an active conformation in the absence of coactivator, whereas in human APC/C coactivators induce a conformational change of APC2:APC11 from a downwards state, in which the E2-binding site is blocked, to an upwards state competent to bind E2 (Chang, Zhang et al. 2014). Also unknown is the degree of conservation of the mechanism of APC/C^{CDC20} activation by APC/C phosphorylation. In human APC/C, phosphorylation of an autoinhibitory (AI) segment incorporated within a long loop of the APC1 subunit removes a steric blockade to the binding of the CDC20 C-box to its binding site on APC8 (Fujimitsu, Grimaldi et al. 2016, Qiao, Weissmann et al. 2016, Zhang, Chang et al. 2016). In our *S. cerevisiae* apo-APC/C cryo-EM maps we observe no evidence of an auto-inhibitory segment bound to the coactivator C box-binding site in APC8. Thus it seems likely that mechanisms of activation of APC/C^{CDC20} by phosphorylation are not conserved from *S. cerevisiae* to human. Here, we present a comparative study of human and *S. cerevisiae* APC/C.

Results

Overall structure of *S. cerevisiae* APC/C complexes

We reconstituted *S. cerevisiae* APC/C using the baculovirus/insect cell system (Zhang, Yang et al. 2016) (**Supplementary Fig. 1a**), similar to methods described previously (Schreiber, Stengel et al. 2011). When in complex with the CDH1 coactivator, the reconstituted APC/C ubiquitylated the high-affinity *S. cerevisiae* substrate Hsl1 (**Supplementary Fig. 1b, c**). Phosphorylated APC/C was generated using CDK2-cyclin A, and mass spectrometry revealed the majority of phosphosites mapped to the APC1, APC3 and APC6 subunits (**Supplementary Table 1**). We prepared cryo-EM grids for three APC/C complexes; (i) a ternary APC/C$^{CDH1:Hsl1}$ complex, (ii) apo-APC/C and (iii) phosphorylated apo-APC/C (**Supplementary Figs 2, 3**). A cryo-EM reconstruction of the ternary APC/C$^{CDH1:Hsl1}$ complex was determined at 4 Å, whereas the structures of unphosphorylated and phosphorylated apo-APC/C were determined at 4.9 Å and 4.5 Å resolution, respectively (**Figs 1-3, Supplementary Figs 2-6 and Supplementary Table 2**). We built the atomic coordinates based on prior structures of human (Chang, Zhang et al. 2015, Höfler, Yu et al. 2024), *E. cuniculi* (Zhang, Roe et al. 2010), *S. cerevisiae* (Au, Leng et al. 2002) and *S. pombe* (Zhang, Kulkarni et al. 2010, Zhang, Chang et al. 2013) APC/C subunits, and used AlphaFold2 predictions (Jumper, Evans et al. 2021, Tunyasuvunakool, Adler et al. 2021) to guide *de novo* model building (**Supplementary Table 3**). The overall structure of the recombinant APC/C$^{CDH1:Hsl1}$ ternary complex is similar to the 10 Å resolution cryo-EM structure of APC/C$^{CDH1:Hsl1}$ reconstituted using native APC/C purified from endogenous sources (da Fonseca, Kong et al. 2011), and our earlier negative stain EM reconstruction (Schreiber, Stengel et al. 2011). The complex adopts a triangular structure delineated by a lattice-like shell that generates a central cavity. The APC/C is comprised of two major modules; the TPR lobe composed of the canonical TPR subunits APC3/CDC27, APC6/CDC16 and APC8/CDC23, and the platform module composed of the large APC1 subunit, together with APC4 and APC5. The TPR lobe adopts a quasi-symmetric structure through the sequential stacking of the three structurally-related TPR homo-dimers, APC8/CDC23, APC6/CDC16 and APC3/CDC27. Each TPR protein is composed of 12-13 copies of the TPR motif, a 34-residue repeat that forms a pair of anti-parallel α-helices. Consecutive arrays of TPR motifs fold into a TPR superhelical structure with a pitch of seven TPR motifs (Das, Cohen et al. 1998). The TPR helix defines an inner TPR groove suitable for protein binding. Each of the three TPR proteins of the TPR lobe homo-dimerise through their N-terminal TPR helix. The two C-

terminal TPR helices of the APC3 homo-dimer provide the IR-tail binding site for coactivators and APC10 (Matyskiela and Morgan 2009, Chang, Zhang et al. 2014, Chang, Zhang et al. 2015), whereas structurally equivalent sites on APC8 interacts with the C-box of coactivator N-terminal domains (NTDs) (Chang, Zhang et al. 2015), and also with the IR tail of the the CDC20 subunit of the mitotic checkpoint complex (MCC^{CDC20}) of the APC/C^{MCC} complex (Alfieri, Chang et al. 2016, Yamaguchi, VanderLinden et al. 2016). Assembly of the complete APC/C complex is augmented by four small non-globular intrinsically disordered proteins (IDPs) that by interacting simultaneously with multiple large globular subunits stabilise the APC/C.

Together, the platform and TPR modules create a scaffold for the juxtaposition of the catalytic and substrate recognition modules, with the catalytic module of the cullin subunit APC2 and the RING-domain subunit APC11 binding to the platform module. Two subunits mediate substrate recognition through a substrate-recognition module: the exchangeable coactivator subunits (CDC20, CDH1 and Ama1) and the core APC/C subunit APC10. Coactivators and APC10 share in common a conserved C-terminal IR (Ile-Arg) tail that each interacts with the symmetry-related subunits of the APC3 homo-dimer. Additionally, APC10 interacts with APC1, and the NTDs of coactivators interact with both the TPR and platform modules. Cryo-EM density bridging the CDH1 WD40 domain ($CDH1^{WD40}$) and APC10 corresponds to the D-box degron of Hsl1 (da Fonseca, Kong et al. 2011). In all three states, the APC2:APC11 catalytic module adopts an upward conformation that positions the APC11 RING domain ($APC11^{RING}$) proximal (~30 Å) to the substrate (**Figs 1-3**), similar to that observed in the active human $APC/C^{CDH1:EMI1}$ complex (**Fig. 4a, b**) (Chang, Zhang et al. 2015, Höfler, Yu et al. 2024).

Detailed subunit analysis

APC2

A recent analysis of human $APC/C^{CDH1:EMI1}$ determined at 2.9 Å resolution revealed a zinc-binding module ($APC2^{ZBM}$) inserted within cullin repeat 2 (CR2) of APC2 (Höfler, Yu et al. 2024). This segment constitutes a 45-residue insert between the A and B α-helices of CR2 (**Fig. 5a**), and is most similar in structure to treble-clef/GATA-like zinc fingers. Four Cys residues coordinate the zinc ion in human APC2. A multiple sequence alignment showed that $APC2^{ZBM}$ is conserved within metazoan APC2 sequences (from humans to *C. elegans*), but not in yeast APC2 sequences (Chang, Zhang et al. 2015, Höfler, Yu et al. 2024). Consistent with this analysis, there is no structural equivalent of human $APC2^{ZBM}$ in the cryo-EM structure of *S. cerevisiae* $APC/C^{CDH1:Hsl1}$ (**Fig. 5b, c**). $APC2^{ZBM}$ substantially increases the thermal stability of human APC2. Whether it performs additional roles is unknown.

Similarly to human APC/C structures, the C-terminal domain (CTD) of APC2 ($APC2^{CTD}$), together with the associated APC11 subunit, are less well defined than other regions of the complex, with the WHB domain of APC2 ($APC2^{WHB}$) being highly flexible and not visible in cryo-EM density (**Fig. 1a and Supplementary Fig. 3e**). In human APC/C structures, $APC2^{WHB}$ is likewise flexible when not in complex with the priming E2 (UbcH10) or bound to the MCC (Brown, VanderLinden et al. 2015, Chang, Zhang et al. 2015). $APC2^{WHB}$ becomes ordered when the APC/C forms complexes with either UbcH10 (Brown, VanderLinden et al. 2015), the MCC (Alfieri, Chang et al. 2016, Yamaguchi, VanderLinden et al. 2016), Nek2A (Alfieri, Tischer et al. 2020), or SUMOylated (Yatskevich, Kroonen et al. 2021).

APC4

The APC4 subunit comprises a WD40 domain with a long four-helix bundle insert between blades 3 and 4, augmented by an insert within blade 3 that is an α-helix in human APC4 and a β-hairpin in *S. cerevisiae* APC4 (**Fig. 5d, e**). Strikingly, in contrast to human APC4 which incorporates a typical seven-β-bladed propeller, in *S. cerevisiae* the APC4 WD40 domain ($APC4^{WD40}$) is constructed from six blades (blades 1-6) (**Fig. 5d**). The absence of cryo-EM density for a blade7 in *S. cerevisiae* APC4 is supported by an AlphaFold2 prediction (Tunyasuvunakool, Adler et al. 2021) (**Fig. 5f, g**). The

predicted APC4 model includes an α-helix instead of blade7. However, this helix is not supported by corresponding cryo-EM density, and is a low confidence prediction based on a low pLDDT score (**Fig. 5f, g**). The unusual APC4^{WD40} domain architecture might be specific to *S. cerevisiae*. The AlphaFold2 prediction of *S. pombe* APC4 proposes a seven-bladed WD40 domain (Tunyasuvunakool, Adler et al. 2021).

Other platform module subunits

APC1: APC1, the largest APC/C subunit (1,748 residues in *S. cerevisiae*), is composed of an N-terminal WD40 β-propeller domain (APC1^{WD40}) and a toroidal PC domain (proteosome/cyclosome) (APC1^{PC}) interconnected by a predominantly α-helical solenoid domain (APC1^{Mid}) (**Supplementary Fig. 7**). APC5 comprises an N-terminal α-helical domain and C-terminal TPR domain of 13 TPR motifs generating two TPR helical turns. APC10 is a DOC homology domain comprising a β-sandwich homologous to galactose-binding domains (Wendt, Vodermaier et al. 2001, Au, Leng et al. 2002).

Structure of intrinsically disordered regions and intrinsically disordered proteins

Our structure indicates how the four smaller non-globular subunits (APC9, CDC26/APC12, SWM1/APC13, MND2) (Zachariae, Shin et al. 1996, Zachariae, Shevchenko et al. 1998, Hall, Torres et al. 2003, Passmore, McCormack et al. 2003), with a high content of intrinsically disordered regions (IDRs), mediate inter-subunit interactions between the larger globular subunits (**Fig. 4**). CDC26/APC12 and SWM1/APC13 share sequence conservation with their metazoan counterparts (Schwickart, Havlis et al. 2004) (**Supplementary Table 3**), consistent with the proposal that SWM1 is the ortholog of metazoan APC13 (Hall, Torres et al. 2003, Passmore, McCormack et al. 2003). MND2 and APC9 share no clear sequence similarities with metazoan APC/C subunits, although previous structure-based mapping of MND2 and APC9 to the *S. cerevisiae* APC/C EM-reconstruction suggested counterparts to APC15 and APC16, respectively (Schreiber, Stengel et al. 2011), consistent with the proposal that MND2 is the *S. cerevisiae* ortholog of human APC15 (Mansfeld, Collin et al. 2011), and that MND2 and APC15 share related functions in promoting the auto-ubiquitylation of CDC20 in the context of the *S. cerevisiae* and human APC/C:MCC complexes (Mansfeld, Collin et al. 2011, Foster and Morgan 2012, Uzunova, Dye et al. 2012, Alfieri, Chang et al. 2016). Analysis of the subunit composition of APC/C complexes purified from *S. cerevisiae* strains harbouring specific gene deletions revealed that APC9 is required for the efficient incorporation of CDC27/APC3 into the assembled APC/C (Zachariae, Shevchenko et al. 1998, Passmore, McCormack et al. 2003), whereas SWM1/APC13 and CDC26/APC12 are required for the stoichiometric assembly of APC3, APC6 and APC9 into the complex (Zachariae, Shevchenko et al. 1998, Schwickart, Havlis et al. 2004). MND2 deletion did not affect the association of other subunits (data not shown from (Schwickart, Havlis et al. 2004)).

CDC26/APC12

The N-terminal 13 residues of CDC26/APC12 insert into the TPR groove of APC6, adopting an extended conformation and mode of binding highly conserved with previous cryo-EM and crystallographic structures of human and *S. pombe* orthologs (Wang, Dye et al. 2009, Zhang, Kulkarni et al. 2010, Chang, Zhang et al. 2014, Chang, Zhang et al. 2015) (**Fig. 4**), although at the resolution of our APC/C$^{CDH1:Hsl1}$ cryo-EM map we cannot define an N-terminal acetyl group visualised in the crystal structure of the *S. pombe* APC6-APC12 complex (Zhang, Kulkarni et al. 2010). CDC26/APC12 then folds into an α-helix that packs against α-helices of the inner groove of the APC6 TPR super-helix, similar to the human and *S. pombe* APC6:APC12 complexes, as is the disordered C-terminus of CDC26/APC12. In neither the human and *S. cerevisiae* APC/C complexes, apart from APC6, do we observe interactions of CDC26/APC12 with other APC/C subunits. Thus, the role of CDC26/APC12 in stabilising the association of APC3, APC6 and APC9 with the APC/C complex (Zachariae, Shevchenko et al. 1998, Schwickart, Havlis et al. 2004) is likely through its specific role in stabilising the APC6 TPR super-helix (Wang, Dye et al. 2009) which bridges APC3 with APC8 (**Fig. 4e, f**)

SWM1/APC13
In human APC/C, the APC13 N-terminus inserts into the TPR groove formed by the N-terminal TPR helix of APC8A (Chang, Zhang et al. 2014, Brown, VanderLinden et al. 2015, Chang, Zhang et al. 2015). The extended chain of APC13 then interacts with structurally equivalent symmetry-related shallow grooves present on the outer TPR-helical ridges of APC8B, APC6A, APC6B and APC3A (sites 4-7, **Fig. 4f**). These shallow grooves are lined with side chains of aromatic residues that engage hydrophobic residues of APC13 (Chang, Zhang et al. 2015). This pattern of TPR subunit engagement by APC13 is continued by APC16 interactions with equivalent sites on APC3B, APC7A and APC7B (sites 1-3, **Fig. 4f**). An earlier electron microscopy analysis of *S. cerevisiae* APC/C using an APC13-green fluorescent protein fusion positioned APC13 close to the APC6-APC3 interface (Schreiber, Stengel et al. 2011), correlating with the position of human APC13. In our structure of *S. cerevisiae* APC/C$^{CDH1:Hsl1}$, we built APC13 into discontinuous cryo-EM density that spans APC8 to APC3. Similar to human APC13, *S. cerevisiae* APC13 engages the structurally equivalent sites on APC8B, APC6A, APC6B and APC3B (sites 4-7, **Fig. 4e**), with its N-terminus also inserting into the TPR groove of APC8A.

Human APC13 and *S. cerevisiae* SWM1/APC13 perform comparable structural roles, contacting the successive TPR subunits of the TPR lobe. We proposed previously that these contacts function to order the stacking of TPR homo-dimers of the TPR groove by breaking the symmetry of inter-TPR dimer interfaces. Although human and *S. cerevisiae* APC13 share only low sequence similarity (**Supplementary Table 3**), their conserved structural roles presumably explains the ability of human APC13 to substitute for the function of *S. cerevisiae* SWM1/APC13 *in vivo* (Schwickart, Havlis et al. 2004, Penkner, Prinz et al. 2005).

APC9 (human APC16 ortholog)
In human APC/C, APC16 is visible as a single 40-residue extended α-helix that lies along the shallow grooves on the outer TPR-helical ridges of APC3B, APC7A and APC7B, forming equivalent interactions as observed for APC13 contacts with APC3, APC6 and APC8 (Chang, Zhang et al. 2014, Brown, VanderLinden et al. 2015, Chang, Zhang et al. 2015) (**Fig. 4f**). *S. cerevisiae* APC9 is over twice the size of APC16 with the two proteins sharing no clear sequence similarity. Based on a subunit deletion approach, we had previously assigned a region of APC9 to the C-terminal TPR super-helix of APC3A (Schreiber, Stengel et al. 2011). This clearly differs from the association of APC16 with human APC/C. Guided by an AlphaFold2 prediction of APC9 (Tunyasuvunakool, Adler et al. 2021) and a complex of APC9 and APC3 (Jumper, Evans et al. 2021), we built 131 of 265 residues into the *S. cerevisiae* APC/C$^{CDH1:Hsl1}$ cryo-EM map as three discontinuous segments (**Fig. 4c and Supplementary Table 3**). The C-terminal segment (segment 3) is a short three-turn α-helix that is structurally homologous to the mode of human APC16 binding to APC3B (**Fig. 4e, f**). Segment 2, composed of three separated α-helices, docks onto the outer surface of APC3A, bridging the two turns of the TPR helix (**Fig. 4e**). Finally, segment 1 bridges APC3A and APC6A (**Fig. 4c insert**), likely explaining why APC9 deletion causes loss of both APC3 and APC9 from purified APC/C complexes (Zachariae, Shevchenko et al. 1998, Passmore, McCormack et al. 2003).

MND2/APC15
In human APC/C, the visible regions of APC15 adopt a relatively simple elongated structure, with the N-terminus of the protein inserting as an extended chain into the groove formed by the N-terminal TPR helix of APC5, then forming an α-helix (APC15^{NTH}) that contacts the N-terminal α-helical domain of APC5, before engaging a groove at the interface of APC6A and APC8A. APC15 interacts with APC8A at a site structurally equivalent to the sites on APC8B, APC6 and APC3 engaged by the other small subunits APC9/APC16, APC12, and APC13 (site 8, **Fig. 4b, d and f**). *S. cerevisiae* MND2/APC15 also contacts the N-terminal α-helical domain of APC5, and APC6A and APC8A, as for human APC15, but has an overall more irregular structure, with its N-terminus docking into a groove formed between the APC5 TPR helix and the four-helical bundle of APC4 (**Fig. 4a, c and e**). In

contrast to human APC5, the APC5 TPR groove is occupied by a loop emanating from the APC5 N-terminal α-helical domain. An insert of *S. cerevisiae* APC15, not conserved in human, protrudes into the APC/C cavity, engaging the outer TPR helix of APC8B that forms the C-box binding site (**Fig. 4a**). A stretch of ~40 acidic residues, common to both human and *S. cerevisiae* APC15, is C-terminal to the ordered regions of APC15 in both complexes.

In the human APC/C^{MCC} structure, the mitotic checkpoint complex (MCC) was observed to adopt both closed and open conformations (APC/C^{MCC}-closed and APC/C^{MCC}-open), with APC/C^{MCC}-closed being associated with disorder of APC15^{NTH} and concomitant conformational changes of APC4 and APC5, whereas an ordered APC15^{NTH} is associated with APC/C^{MCC}-open (Alfieri, Chang et al. 2016, Yamaguchi, VanderLinden et al. 2016). In APC/C^{MCC}-closed, the UbcH10-binding site on the APC2:APC11 catalytic module is sterically occluded by the MCC. These structural observations explained why APC15 deletion in human APC/C abolished CDC20^{MCC} auto-ubiquitylation in the context of APC/C^{MCC} (Uzunova, Dye et al. 2012, Alfieri, Chang et al. 2016, Yamaguchi, VanderLinden et al. 2016). Our observation that APC15^{NTH} is structurally conserved in *S. cerevisiae* APC/C is consistent with a defect in CDC20^{MCC} ubiquitylation caused by deleting APC15 (Foster and Morgan 2012). In contrast to MND2/APC15 promoting CDC20^{MCC} ubiquitylation during the SAC, in *S. cerevisiae*, MND2 specifically suppresses securin/Pds1 ubiquitylation by the Ama1 coactivator-APC/C complex that prevents premature sister chromatid segregation during meiosis (Oelschlaegel, Schwickart et al. 2005). The 14 sites of MND2 phosphorylation required for efficient APC/C^{Ama1}-regulated progression through meiosis I (Torres and Borchers 2007), are located within, and C-terminal to, the acidic stretch in MND2, and are therefore not visible in our structure.

A common feature of all the small APC/C subunits is that they form extended, mainly irregular structures, that simultaneously contact multiple large globular APC/C subunits. CDC26/APC12, SWM1/APC13 and human APC15 are anchored at their N-termini by inserting into the TPR grooves of APC6, APC8A and APC5, respectively. These interactions serve to stabilise the TPR groove through formation of protein-protein interactions (Wang, Dye et al. 2009). In human APC/C, a 40-residue loop of APC1^{WD40} inserts into the TPR groove of APC8B, although this structural feature is not conserved in *S. cerevisiae* APC/C.

<u>Interactions of CDH1 with APC/C and conserved regulation by phosphorylation</u>
Coactivators interact with the APC/C through an N-terminal C-box motif (Schwab, Neutzner et al. 2001) and a C-terminal IR tail (Passmore, McCormack et al. 2003, Vodermaier, Gieffers et al. 2003). Both motifs are highly evolutionarily conserved. Interestingly, although the seven-residue C-box and two-residue IR tail lack obvious sequence similarity, the C-box binding site within the TPR helix of APC8B is structurally conserved with the IR-tail binding site on APC3, with an Arg residue, common to both, anchoring the motifs to their respective binding sites (Chang, Zhang et al. 2015). The docking of the coactivator C-box motif to this site on APC8B/CDC23 rationalises the temperature-sensitive cell cycle mutations of *S. cerevisiae CDC23* (Sikorski, Boguski et al. 1990), and prior mutagenesis data implicating Asn405 of APC8/CDC23 in CDH1 binding (Matyskiela and Morgan 2009). Additionally, other segments within CDH1^{NTD} mediate APC/C-coactivator interactions. When in complex with the APC/C, CDH1^{NTD} folds into five α-helices (labelled α2-α6) (**Fig. 6**). Four of these α-helices mediate APC/C – CDH1 interactions, three of which; α2, α3 and α6, that form anti-parallel interactions with APC1^{PC} α-helices, being conserved with human CDH1 (**Fig. 6b, e**). Unique to *S. cerevisiae* CDH1 is a three-turn α-helix (α5) that docks onto the outer TPR ridge of APC6B, running antiparallel to exposed α-helices, and bridging APC8B (**Fig. 6a, c**). CDK phosphorylation of CDH1^{NTD} inhibits CDH1 binding to the APC/C, and substituting alanines for all eleven predicted CDK sites in *S. cerevisiae* CDH1 almost completely eliminated CDH1 phosphorylation in mitosis (Zachariae, Schwab et al. 1998). Mimicking six CDK phosphosites with aspartates abolished binding of CDH1 to the APC/C *in vivo*, whereas a mutant with non-phosphorylatable sites bound APC/C more tightly than wild type CDH1 (Hockner, Neumann-Arnold et al. 2016). Five of these CDK sites, with additional non-

consensus CDK sites, were reported to be phosphorylated *in vivo* (Hall, Warren et al. 2004). Mapping these phosphosites onto the *S. cerevisiae* APC/C$^{CDH1:Hsl1}$ structure suggested a rationale for how CDH1^{NTD} phosphorylation inhibits binding of CDH1 to the APC/C (**Fig. 6a**). Two CDK sites (Ser227, Ser239) are conserved in human CDH1 (**Fig. 6b**) (Chang, Zhang et al. 2015), and map on or close to the α6 helix that docks onto APC1^{PC} (**Fig. 6a**). Phosphorylation of either site in human CDH1 contributed significantly to CDH1 inactivation (Chang, Zhang et al. 2015), likely by disrupting CDH1^{NTD}-APC1^{PC} interactions. Thus, this analysis reveals an evolutionarily conserved molecular mechanism for inhibiting CDH1 binding to the APC/C through CDK phosphorylation. Additionally, three reported non-consensus CDK-phosphosites within α5 (Ser216, Ser220, Ser225) (Hall, Warren et al. 2004) would likely interfere with α5 interactions with APC6B and APC8B (**Fig. 6a**).

The recent 2.9 Å resolution cryo-EM structure of APC/C$^{CDH1:EMI1}$ revealed an N-terminal amphipathic α-helix of CDH1 (CDH1$^{\alpha1}$) interacting through non-polar interactions with a hydrophobic groove in the APC1^{WD40} domain (Höfler, Yu et al. 2024). This α-helix is conserved in metazoan coactivators, but consistent with MSA analysis, is not present in *S. cerevisiae* CDH1.

Finally, the mode of binding of CDH1^{IR} to the IR-tail binding site on APC3A is conserved with that of human APC/C$^{CDH1:EMI1}$ (Matyskiela and Morgan 2009, Brown, VanderLinden et al. 2015, Chang, Zhang et al. 2015, Höfler, Yu et al. 2024) (**Fig. 7a-d**). In *S. cerevisiae* APC/C, the interaction of APC9 with APC3A (segment 2 of APC9) and APC3B (segment 3 of APC9) partially mimics the respective APC7 and APC16 interactions with human APC3 (**Fig. 7e, f**). APC9 segment 2 interactions with the C-terminal TPR helix of APC3A may stabilise the CDH1^{IR} tail-binding site of APC3A.

<u>Comparison of apo-APC/C with APC/C$^{CDH1:Hsl1}$</u>

Biochemical studies on both metazoan (*Xenopus*) and *S. cerevisiae* APC/C revealed that coactivators function as substrate adaptors (Burton and Solomon 2001, Hilioti, Chung et al. 2001, Schwab, Neutzner et al. 2001, Kraft, Vodermaier et al. 2005), and also enhance APC/C catalytic activity (Kimata, Baxter et al. 2008, Van Voorhis and Morgan 2014). For *S. cerevisiae* APC/C, catalytic enhancement results from a substantially more efficient interaction of the APC/C with its E2s Ubc4 and Ubc1 (Van Voorhis and Morgan 2014). Similarly, the affinity of the human APC/C for UbcH10 is increased three-fold when in complex with CDH1 (Chang, Zhang et al. 2014). In human APC/C, the association of CDH1 induces a conformational change of the APC2:APC11 catalytic module from a downwards state, in which the UbcH10-binding site is blocked, to an upwards state competent to bind UbcH10 (Chang, Zhang et al. 2014). Comparing unphosphorylated *S. cerevisiae* apo-APC/C and APC/C$^{CDH1:Hsl1}$ showed that in both states the APC2:APC11 catalytic module adopts the same raised position (**Fig. 8a, b**), similar to human APC/C$^{CDH1:EMI1}$. Docking Ubc4 onto the RING domain of APC11 (based on the *S. cerevisiae* Not4:Ubc4 coordinates; PDB 5AIE (Bhaskar, Basquin et al. 2015)) indicated that the conformation of the APC2:APC11 catalytic module in apo-APC/C does not sterically occlude Ubc4 binding (**Fig. 8c, d**). Thus, the mechanism by which coactivator stimulates *S. cerevisiae* APC/C catalytic activity through enhancing E2 binding differs from human APC/C, although the structural mechanism is not defined in our study.

Why isn't *S. cerevisiae* apo-APC/C in an inactive conformation? The interaction of CDH1^{NTD} with APC1 and APC8B of human APC/C explains how CDH1 association promotes a conformational change of the APC/C that results in the upward movement of the APC2:APC11 catalytic module (Chang, Zhang et al. 2014, Höfler, Yu et al. 2024). In the human ternary complex, CDH1^{NTD} disrupts the interaction between APC1^{PC} and APC8B by binding to a site on APC1^{PC} that overlaps the site in contact with APC8B. This wedges APC1^{PC} and APC8B apart. The resultant downwards-displacement of APC8B tilts the platform to translate the APC2^{CTD}:APC11 module upwards. In contrast to human APC/C, in the more open structure of *S. cerevisiae* apo-APC/C, the TPR lobe does not directly contact APC1^{PC}, and thus the position of APC8B relative to the APC8B – CDH1^{NTD1}-binding site does not impede CDH1 association. Instead, on binding to *S. cerevisiae* APC/C, of CDH1^{NTD} interconnects

the TPR lobe with APC1^{PC} to reinforce TPR and platform lobe interactions (**Fig. 8a, b;** lower panels). To accommodate closure of the APC/C cavity, conformational changes are distributed over the subunits of the TPR and platform lobes, including a tilt of APC1^{PC} relative to the combined domains of APC1^{Mid}-APC1^{WD40} (**Supplementary Figure 7 and Supplementary Video 1**).

Mechanism of APC/C activation by phosphorylation

Hyperphosphorylation of APC/C subunits APC1 and APC3 is required for CDC20 to activate the APC/C (Lahav-Baratz, Sudakin et al. 1995, Shteinberg, Protopopov et al. 1999, Kramer, Scheuringer et al. 2000, Rudner and Murray 2000, Golan, Yudkovsky et al. 2002, Kraft, Vodermaier et al. 2005, Fujimitsu, Grimaldi et al. 2016, Qiao, Weissmann et al. 2016, Zhang, Chang et al. 2016). In metazoan unphosphorylated apo-APC/C, an auto-inhibitory (AI) segment incorporated into the 300s loop inserted within the WD40 domain of APC1 (APC1^{300L}) sterically occludes the C-box binding site on APC8B (APC8$^{C\text{-}box}$) thereby competing for CDC20 binding (Fujimitsu, Grimaldi et al. 2016, Qiao, Weissmann et al. 2016, Zhang, Chang et al. 2016). Phosphorylation of residues within (APC1^{300L}), including the AI segment, displaces the AI segment from APC8$^{C\text{-}box}$ allowing CDC20 binding. Multiple lines of data support this model, including the observation of cryo-EM density for the AI segment bound to APC8$^{C\text{-}box}$ (Zhang, Chang et al. 2016, Höfler, Yu et al. 2024), the constitutive activation of APC/C^{CDC20} on deleting APC1^{300L}, and the location of multiple CDK and PLK1 sites within APC1^{300L} (Fujimitsu, Grimaldi et al. 2016, Li, Chang et al. 2016, Qiao, Weissmann et al. 2016, Zhang, Chang et al. 2016, Höfler, Yu et al. 2024). Replacing these phosphosites with glutamates activated APC/C^{CDC20}, whereas in contrast, mutations to Ala prevented CDK activation of APC/C^{CDC20} (Fujimitsu, Grimaldi et al. 2016, Qiao, Weissmann et al. 2016, Zhang, Chang et al. 2016, Höfler, Yu et al. 2024). Our cryo-EM structure suggests that activation of *S. cerevisiae* APC/C^{CDC20} by phosphorylation operates by a different mechanism. We observe no cryo-EM density occupying the C-box binding site of APC8B (**Fig. 9a, b**). Arguably, the low resolution of the unphosphorylated apo-APC/C structure means that we cannot definitively state that APC8$^{C\text{-}box}$ is not occluded in the unphosphorylated apo-state. However, the Morgan lab recently reported that deleting the APC1 WD40 loop of *S. cerevisiae* (residues 225-365), equivalent to human APC1^{300L}, caused only a minor growth defect, but importantly no evidence for APC/C hyperactivation (Ng, Adly et al. 2024), a finding that is not consistent with a model in which *S. cerevisiae* and human APC/C share a common phospho-regulatory mechanism.

Superimposing both apo-APC/C states (phosphorylated and unphosphorylated) reveals that the only obvious difference between the two is a small relative shift of the TPR lobe (**Fig. 9c-e**). Since APC/C phosphorylation stimulates CDC20 association, and not CDH1, we would expect specific and perhaps localised conformational changes in the APC/C. It is possible that in contrast to the activation of human APC/C^{CDC20} through release of a negative auto-inhibitory segment, phosphorylated regions of *S. cerevisiae* APC/C might contact CDC20 directly or indirectly to enhance its binding. We note that 'unphosphorylated' APC/C isolated from insect cells is partially phosphorylated prior to its treatment with CDK2 (**Supplementary Table 1**). Although CDK2-dependent phosphorylation causes the expected mobility shift in APC3/CDC27 (**Supplementary Fig. 1a**), and an increase in phosphorylation sites (**Supplementary Table 1**), it is possible that 'unphosphorylated' APC/C may already containctivating phosphorylation sites, thus explaining the absence of conformational change on *in vitro* CDK2-mediated phosphorylation. Our phosphoproteomic study did not assess phospho-site stoichiometry.

Discussion

We present a comparative study of human and *S. cerevisiae* APC/C. This revealed a similar overall architecture, with the largest difference being the absence of an APC7 homolog in *S. cerevisiae*. A recent study discovered a specific role for APC7 in mammalian brain development (Ferguson, Urso et al. 2022). Homozygous ANAPC7 mutations in humans, leading to loss of APC7 protein, underlies an

inherited intellectual disability syndrome, caused by defective APC/C$^{\Delta APC7}$-mediated degradation of the chromosome-associated protein Ki-67 (Ferguson, Urso et al. 2022). Thus in mammals, APC7 confers specific post-mitotic functions in the developing brain through selective protein-recognition. The mode of binding of the CDH1 coactivator subunit is also very similar, except for the presence in human APC/C of the N-terminal α-helix (CDH1$^{\alpha 1}$), not conserved in *S. cerevisiae* APC/C, that mediates contacts to APC1^{WD40}. Also conserved is the mechanism of inactivation of CDH1 by CDK phosphorylation of two conserved serine residues on CDH1 at the CDH1^{NTD} – APC1^{PC} interface. Major differences between human and *S. cerevisiae* APC/C are how coactivators enhance APC/C affinity for E2s (UbcH10 in human (Chang, Zhang et al. 2014), Ubc1 and Ubc4 in *S. cerevisiae* (Van Voorhis and Morgan 2014)), and how APC/C^{CDC20} is activated by CDK-mediated APC/C phosphorylation. What is clear from our structural analysis is that unlike human APC/C, in the apo-state of *S. cerevisiae* APC/C, the E2-binding site on APC11^{RING} is accessible, and that CDH1 does not promote a substantial conformational change of the APC2:APC11 catalytic module. However, how CDH1 enhances E2 affinity for APC/C isn't clear from a comparison of the apo-APC/C and APC/C$^{CDH1:Hsl1}$ ternary structures. It is likely that the structures of APC/C$^{CDH1:Hsl1}$ in complex with E2s would reveal this mechanism. Finally, the mechanism of stimulating CDC20-binding to the APC/C through phosphorylation-dependent relief of an auto-inhibitory segment of APC1, as in human APC/C (Fujimitsu, Grimaldi et al. 2016, Qiao, Weissmann et al. 2016, Zhang, Chang et al. 2016), is not conserved in *S. cerevisiae* APC/C, a structural finding that is consistent with *in vivo* data (Ng, Adly et al. 2024). Since comparison of all three reported structures did not reveal a likely mechanism, one explanation could be that a phosphorylated region of the APC/C either directly or indirectly contacts CDC20 to enhance its affinity for the APC/C.

Supplementary Tables

Supplementary Table 1. CDK phosphosites of *S. cerevisiae* APC/C

Supplementary Table 2. Cryo-EM data collection, refinement and validation statistics

Supplementary Table 3. Ordered and disordered regions of APC/C subunits

Materials and Methods

Cloning and expression of recombinant *S. cerevisiae* APC/C and CDH1:Hsl1

S. cerevisiae APC/C genes were previously cloned into a modified MultiBac system (Zhang, Yang et al. 2016). Coding sequences for CDH1 and Hsl1$^{667\text{-}872,\ 1k}$ (Hsl1$^{667\text{-}872,\ K672R/\ K683R/\ K701R/\ K701R/\ K710R/\ K747R/\ K760R/\ K785R/\ K788R/\ K796R/\ K812R/\ K825R/\ K827R/\ K840R/\ K843R/\ K851R/\ K852R/\ K860R/\ K861R/\ K869R}$) were cloned into a pU1 vector by USER methodology (Zhang, Yang et al. 2016).

For APC/C expression, Hi-5 cells at a density of 2x10^6 cells/mL were co-infected with two (apo-APC/C) or three (APC/C$^{CDH1:Hsl1}$) pre-cultures of Sf9 cells each pre-infected with one of the recombinant APC/C baculoviruses. APC/C expression was performed for 48 h. Cells were harvested by centrifugation at 1,000 g for 10 min at 4 ºC.

Purification of recombinant *S. cerevisiae* APC/C

All purification steps were carried out at 4 ºC and are the same for the apo-APC/C and the ternary APC/C$^{CDH1:Hsl1}$ complex. The pellets from insect cells were resuspended in lysis buffer [50 mM Tris-HCl (pH 8.3), 200 mM NaCl, 5 % glycerol, 2 mM DTT, 1 mM EDTA, 2 mM benzamidine, 0.5 mM PMSF, 5 units/mL benzonase (Sigma-Aldrich) and Complete EDTA-free protease inhibitor (Roche)]. After sonication, the cell lysate was centrifuged for 60 min at 48,000 g and filtered (0.45 µm). The cleared supernatant was loaded onto a 5 mL Strep-Tactin Superflow Cartridge (Qiagen) at 1 mL/min.

The column was washed with APC/C buffer [50 mM Tris-HCl (pH 8.0), 200 mM NaCl, 5 % (v/v) glycerol, 2 mM DTT, 1 mM EDTA and 2 mM benzamidine]. The recombinant APC/C complex was eluted with the wash buffer supplemented with 2.5 mM desthiobiotin (Sigma-Aldrich). Before loading the elution fractions onto a 6 mL Resource Q anion-exchange column (Cytiva), they were diluted 1.6-fold into buffer A without NaCl [buffer A: 20 mM HEPES (pH 8.0), 120 mM NaCl, 5 % (v/v) glycerol and 2 mM DTT]. The Resource Q column was washed with buffer A and the APC/C was eluted with a gradient of buffer B [20 mM HEPES (pH 8.0), 1 M NaCl, 5 % (v/v) glycerol and 2 mM DTT]. The resulting elution was concentrated to around 3 mg/mL and ultracentrifuged for 10 min at 40,000 g. The soluble supernatant was loaded onto a Superose 6 Increase 3.2/300 column (Cytiva) equilibrated in APC/C gel-filtration buffer [20 mM HEPES (pH 8.0), 150 mM NaCl and 0.5 mM TCEP]. The gel filtration was run on a ÄKTAmicro (Cytiva) with a flow rate of 50 µL/min.

In vitro phosphorylation of recombinant *S. cerevisiae* APC/C

Resource Q apo-APC/C peak fractions were diluted two-fold into buffer A without NaCl and concentrated. The concentrated sample was treated with CDK2–cyclin A3–Cks2 (Zhang, Chang et al. 2016) in a molar ratio of 1:1.5 (APC/C: kinases) in a reaction buffer of 40 mM HEPES (pH 8.0), 10 mM $MgCl_2$, 5 mM ATP, 50 mM NaF, 0.1 µM okadaic acid and 20 mM β-glycerophosphate. The reaction mixture was incubated at 30°C for 30 min. Subsequently, the phosphorylated protein was run on a Superose Increase 6 3.2/300 column (Cytiva) with APC/C gel-filtration buffer [20 mM HEPES (pH 8.0), 150 mM NaCl, 0.5 mM TCEP]. For the ubiquitination assays, the reaction was stopped with 15 µM CDK1/2 Inhibitor III (Calbiochem) without further purification steps.

Ubiquitination assays

APC/C ubiquitination assays were adopted from (Passmore, Barford et al. 2005). ^{35}S-labelled substrates (*S. cerevisiae* Hsl1) and unlabelled *S. cerevisiae* wildtype CDH1 were prepared *in vitro* using the TNT T7 Quick Coupled Transcription/Translation System (Promega). Each reaction contained 60 nM recombinant *S. cerevisiae* APC/C, 0.5 µL of ^{35}S-labelled substrate and 2 µL CDH1 in a 10 µL reaction volume with 40 mM Tris.HCl (pH 7.5), 10 mM $MgCl_2$, 0.6 mM DTT, 5 mM ATP, 150 nM UBA1, 300 nM Ubc4, 70 µM ubiquitin, 200 ng ubiquitin aldehyde (Enzo), and 2 µM LLnL (N-Acetyl-Leu-Leu-Norleu-aldehyde) (Sigma-Aldrich). Reactions were incubated at 30 °C for 2 h and terminated adding SDS/PAGE loading buffer. Samples were analysed by NuPAGE 4-12% Bis-Tris protein gels (ThermoFisher Scientific). Gels were fixed and stained with InstantBlue (Expedeon) followed by drying and exposure to X-ray Film (Photon Imaging Systems).

Electron microscopy

Freshly purified APC/C samples were visualised by negative-staining EM to assess the quality and homogeneity of the sample. Micrographs were recorded on a CryoSpirit electron microscope (ThermoFisher Scientific) at an accelerating voltage of 120 keV and at a defocus of approximately -1.5 µm. For cryo-EM, Quantifoil R3.5/1 grids coated with a layer of continuous carbon film (approximately 50 Å thick) were glow-discharged for 30 s before deposition of 3 µL fresh sample (~0.12 mg/mL), blotted for 8 s, and vitrified by plunging into liquid ethane with a custom-made manual plunger at 4 °C. Micrographs were collected on a Titan Krios microscope (ThermoFisher Scientific) at an acceleration voltage of 300 keV and Falcon III direct electron detector. Micrographs were taken using EPU software (ThermoFisher Scientific) at a nominal magnification of 59,000x, with a calibrated pixel size of 1.38 Å. Fifty nine movie frames with an average electron dose of 59 $e^-/Å^2$ were recorded in integration mode for 1.49 s. The defocus range was set at -2.0 to -4.0 µm.

Image processing

All movie frames were aligned and averaged with MotionCor2 (Zheng, Palovcak et al. 2017) or

RELION's own implementation of the MotionCor2 algorithm (Zivanov, Nakane et al. 2018). Contrast transfer function parameters were calculated with Gctf (Zhang 2016). Particles were automatically selected by template-free particle picking in Gautomatch (developed by Kai Zhang, http://www.mrc-lmb.cam.ac.uk/kzhang/Gautomatch/). All subsequent steps were performed in RELION-2/3 (Zivanov, Nakane et al. 2018). Sorting of particle images was performed by 2D and 3D classification, using 60 Å low-pass filtered human unphosphorylated apo-APC/C EM map (EMD-3386) (Zhang, Chang et al. 2016) as an initial 3D reference. The reconstruction generated from all the corresponding *S. cerevisiae* particles, low-pass filtered at 40 Å, was used as a subsequent reference. Finally, the data set was subject to either particle polishing or Bayesian particle polishing (Zivanov, Nakane et al. 2018), CTF refinement and an extra 3D classification step to discard remaining bad particles. All resolution estimations were based on the gold-standard Fourier shell correlation (FSC) calculations using the FSC = 0.143 criterion. **Supplementary Data Table 2** summarises EM reconstructions obtained in this work.

To improve map resolution, multi-body refinement was performed in in RELION 3.0 (Nakane, Kimanius et al. 2018). For the APC/C$^{CDH1:Hsl1}$ reconstruction, three masks were generated: mask 1 encompassed the TPR lobe (APC3, APC6, APC8, APC9, APC13); mask 2 included the platform (APC1, APC4, APC5, APC10, APC15 and CDH1 subunits and Hsl1), mask 3 surrounded the APC2:APC11 catalytic module. The resultant maps were determined at 4.1 Å, 4.06 Å and 7.36 Å, respectively. For the apo-APC/C and phosphorylated apo-APC/C, two masks were used: mask1 contained the TPR lobe subunits; mask 2 included the platform and catalytic subunits. The apo-APC/C maps achieved resolutions of 4.9 Å and 4.58 Å, respectively, whereas the phosphorylated apo-APC/C maps have resolutions of 4.18 Å and 4.23 Å, respectively. The maps obtained from multi-body refinement demonstrated significantly improved definition of cryo-EM densities which facilitated model building.

Model building of APC/C

Model building of the apo-APC/C, APC/C$^{CDH1:Hsl1}$ structures and phosphorylated apo-APC/C were performed in COOT (Emsley and Cowtan 2004). Initially, available atomic structure of human unphosphorylated apo-APC/C (5G05) (Zhang, Chang et al. 2016) and human APC/C$^{CDH1:EMI1}$ (4UI9) (Chang, Zhang et al. 2015) and prior structures of human (Chang, Zhang et al. 2015, Höfler, Yu et al. 2024), *E. cuniculi* (Zhang, Roe et al. 2010), *S. cerevisiae* (Au, Leng et al. 2002) and *S. pombe* (Zhang, Kulkarni et al. 2010, Zhang, Chang et al. 2013) APC/C subunits were rigid-body fitted as individual subunits into the cryo-EM maps in Chimera (Yang, Lasker et al. 2012). Subsequently, the different human and *S. cerevisiae* APC/C protein subunit sequences were aligned using MUSCLE program (Edgar 2004) and Jalview (Waterhouse, Procter et al. 2009). Based on the multiple alignment results, the amino acids from the human fitted atomic structure were substituted for the corresponding *S. cerevisiae* amino acids using COOT. Finally, all fitted structures were rebuilt according to the cryo-EM map and guided by AlphaFold2 predictions of these subunits (Jumper, Evans et al. 2021, Tunyasuvunakool, Adler et al. 2021). APC9, APC13, APC15, the CDH1^{NTD} and several loop regions not seen in previous structures were built *ab initio*, also guided by AlphaFold2 predictions of these subunits, including a prediction of the APC3:APC9 complex. Real-space refinement was performed in PHENIX (Adams, Afonine et al. 2010) and the refined model was validated using the MolProbity tool (Williams, Headd et al. 2018). Maps and models were visualised with COOT (Emsley and Cowtan 2004), and figures generated using Chimera X (Goddard, Huang et al. 2018). The refinement statistics are summarised in **Supplementary Data Table 2**.

Mass spectrometry

Purified proteins were prepared for mass spectrometric analysis by in solution enzymatic digestion, without prior reduction and alkylation. Protein samples were digested with trypsin or elastase (Promega), both at an enzyme to protein ratio of 1:20. The resulting peptides were analysed by nano-

scale capillary LC-MS/MS using an Ultimate U3000 HPLC (ThermoScientific Dionex) to deliver a flow of approximately 300 nL/min. A C18 Acclaim PepMap100 5 µm, 100 µm Å~ 20 mM nanoViper column (ThermoFisherScientific Dionex), trapped the peptides before separation on a C18 Acclaim PepMap100 3 µm, 75 µm Å~ 250 mM nanoViper column (ThermoFischerScientific Dionex). Peptides were eluted with a 90 min gradient of acetonitrile (2% to 50%). The analytical column outlet was directly interfaced via a nano-flow electrospray ionization source, with a hybrid quadrupole orbitrap mass spectrometer (Q-Exactive Plus Orbitrap, ThermoFischerScientific). LC-MS/MS data were then searched against an in-house LMB database using the Mascot search engine (Matrix Science) (Perkins, Pappin et al. 1999), and the peptide identifications validated using the Scaffold program (Proteome Software Inc.) (Keller, Nesvizhskii et al. 2002). All data were additionally interrogated manually.

Acknowledgements
We are grateful to the LMB EM Facility for help with the EM data collection, J. Grimmett, T. Darling and I. Clayson for computing, M. Skehel and S. Maslen for mass spectrometry and J. Shi for help with insect cell expression. For the purpose of open access, the author has applied a CC BY public copyright license to any Author Accepted Manuscript version arising.

Funding
This work was supported by UKRI/Medical Research Council MC_UP_1201/6 (D.B.) and Cancer Research UK C576/A14109 (D.B.).

Competing interests
Authors declare that they have no competing interests.

Data and materials availability
PDB and cryo-EM maps have been deposited with RCSB and EMDB, respectively. Accession numbers are listed in **Supplementary Table 2**.

Correspondence and requests for materials should be addressed to David Barford.

Author contributions
The project has been conceived by D.B and E.V.-F.
Experiments were performed by E.V.-F., A.E.A., J.Y., P.E., Z.Z. and D.B.
The paper was written by D.B. with input from E.V.-F.

References

Adams, P. D., P. V. Afonine, G. Bunkoczi, V. B. Chen, I. W. Davis, N. Echols, J. J. Headd, L. W. Hung, G. J. Kapral, R. W. Grosse-Kunstleve, A. J. McCoy, N. W. Moriarty, R. Oeffner, R. J. Read, D. C. Richardson, J. S. Richardson, T. C. Terwilliger and P. H. Zwart (2010). "PHENIX: a comprehensive Python-based system for macromolecular structure solution." Acta Crystallogr D Biol Crystallogr **66**(Pt 2): 213-221.
Alfieri, C., L. Chang, Z. Zhang, J. Yang, S. Maslen, M. Skehel and D. Barford (2016). "Molecular basis of APC/C regulation by the spindle assembly checkpoint." Nature **536**(7617): 431-436.
Alfieri, C., T. Tischer and D. Barford (2020). "A unique binding mode of Nek2A to the APC/C allows its ubiquitination during prometaphase." EMBO Rep **21**(6): e49831.
Alfieri, C., S. Zhang and D. Barford (2017). "Visualizing the complex functions and mechanisms of the anaphase promoting complex/cyclosome (APC/C)." Open Biol **7**(11).

Au, S. W., X. Leng, J. W. Harper and D. Barford (2002). "Implications for the ubiquitination reaction of the anaphase-promoting complex from the crystal structure of the Doc1/Apc10 subunit." J Mol Biol **316**(4): 955-968.
Barford, D. (2020). "Structural interconversions of the anaphase-promoting complex/cyclosome (APC/C) regulate cell cycle transitions." Curr Opin Struct Biol **61**: 86-97.
Bhaskar, V., J. Basquin and E. Conti (2015). "Architecture of the ubiquitylation module of the yeast Ccr4-Not complex." Structure **23**(5): 921-928.
Bodrug, T., K. A. Welsh, M. Hinkle, M. J. Emanuele and N. G. Brown (2021). "Intricate Regulatory Mechanisms of the Anaphase-Promoting Complex/Cyclosome and Its Role in Chromatin Regulation." Front Cell Dev Biol **9**: 687515.
Brown, N. G., R. VanderLinden, E. R. Watson, R. Qiao, C. R. Grace, M. Yamaguchi, F. Weissmann, J. J. Frye, P. Dube, S. Ei Cho, M. L. Actis, P. Rodrigues, N. Fujii, J. M. Peters, H. Stark and B. A. Schulman (2015). "RING E3 mechanism for ubiquitin ligation to a disordered substrate visualized for human anaphase-promoting complex." Proc Natl Acad Sci U S A **112**(17): 5272-5279.
Brown, N. G., R. VanderLinden, E. R. Watson, F. Weissmann, A. Ordureau, K. P. Wu, W. Zhang, S. Yu, P. Y. Mercredi, J. S. Harrison, I. F. Davidson, R. Qiao, Y. Lu, P. Dube, M. R. Brunner, C. R. Grace, D. J. Miller, D. Haselbach, M. A. Jarvis, M. Yamaguchi, D. Yanishevski, G. Petzold, S. S. Sidhu, B. Kuhlman, M. W. Kirschner, J. W. Harper, J. M. Peters, H. Stark and B. A. Schulman (2016). "Dual RING E3 Architectures Regulate Multiubiquitination and Ubiquitin Chain Elongation by APC/C." Cell **165**(6): 1440-1453.
Brown, N. G., E. R. Watson, F. Weissmann, M. A. Jarvis, R. VanderLinden, C. R. Grace, J. J. Frye, R. Qiao, P. Dube, G. Petzold, S. E. Cho, O. Alsharif, J. Bao, I. F. Davidson, J. J. Zheng, A. Nourse, I. Kurinov, J. M. Peters, H. Stark and B. A. Schulman (2014). "Mechanism of polyubiquitination by human anaphase-promoting complex: RING repurposing for ubiquitin chain assembly." Mol Cell **56**(2): 246-260.
Burton, J. L. and M. J. Solomon (2001). "D box and KEN box motifs in budding yeast Hsl1p are required for APC-mediated degradation and direct binding to Cdc20p and Cdh1p." Genes Dev **15**(18): 2381-2395.
Burton, J. L. and M. J. Solomon (2007). "Mad3p, a pseudosubstrate inhibitor of APCCdc20 in the spindle assembly checkpoint." Genes Dev **21**(6): 655-667.
Buschhorn, B. A., G. Petzold, M. Galova, P. Dube, C. Kraft, F. Herzog, H. Stark and J. M. Peters (2011). "Substrate binding on the APC/C occurs between the coactivator Cdh1 and the processivity factor Doc1." Nat Struct Mol Biol **18**(1): 6-13.
Cappell, S. D., K. G. Mark, D. Garbett, L. R. Pack, M. Rape and T. Meyer (2018). "EMI1 switches from being a substrate to an inhibitor of APC/C(CDH1) to start the cell cycle." Nature **558**(7709): 313-317.
Carroll, C. W., M. Enquist-Newman and D. O. Morgan (2005). "The APC subunit Doc1 promotes recognition of the substrate destruction box." Curr Biol **15**(1): 11-18.
Carroll, C. W. and D. O. Morgan (2002). "The Doc1 subunit is a processivity factor for the anaphase-promoting complex." Nat Cell Biol **4**(11): 880-887.
Chang, L., Z. Zhang, J. Yang, S. H. McLaughlin and D. Barford (2014). "Molecular architecture and mechanism of the anaphase-promoting complex." Nature **513**(7518): 388-393.
Chang, L., Z. Zhang, J. Yang, S. H. McLaughlin and D. Barford (2015). "Atomic structure of the APC/C and its mechanism of protein ubiquitination." Nature **522**(7557): 450-454.
Chao, W. C., K. Kulkarni, Z. Zhang, E. H. Kong and D. Barford (2012). "Structure of the mitotic checkpoint complex." Nature **484**(7393): 208-213.

Cooper, K. F., M. J. Mallory, D. B. Egeland, M. Jarnik and R. Strich (2000). "Ama1p is a meiosis-specific regulator of the anaphase promoting complex/cyclosome in yeast." Proc Natl Acad Sci U S A **97**(26): 14548-14553.
da Fonseca, P. C., E. H. Kong, Z. Zhang, A. Schreiber, M. A. Williams, E. P. Morris and D. Barford (2011). "Structures of APC/C(Cdh1) with substrates identify Cdh1 and Apc10 as the D-box co-receptor." Nature **470**(7333): 274-278.
Das, A. K., P. W. Cohen and D. Barford (1998). "The structure of the tetratricopeptide repeats of protein phosphatase 5: implications for TPR-mediated protein-protein interactions." Embo J **17**(5): 1192-1199.
Edgar, R. C. (2004). "MUSCLE: a multiple sequence alignment method with reduced time and space complexity." BMC Bioinformatics **5**: 113.
Emsley, P. and K. Cowtan (2004). "Coot: model-building tools for molecular graphics." Acta Crystallogr D Biol Crystallogr **60**(Pt 12 Pt 1): 2126-2132.
Ferguson, C. J., O. Urso, T. Bodrug, B. M. Gassaway, E. R. Watson, J. R. Prabu, P. Lara-Gonzalez, R. C. Martinez-Chacin, D. Y. Wu, K. W. Brigatti, E. G. Puffenberger, C. M. Taylor, B. Haas-Givler, R. N. Jinks, K. A. Strauss, A. Desai, H. W. Gabel, S. P. Gygi, B. A. Schulman, N. G. Brown and A. Bonni (2022). "APC7 mediates ubiquitin signaling in constitutive heterochromatin in the developing mammalian brain." Mol Cell **82**(1): 90-105 e113.
Foster, S. A. and D. O. Morgan (2012). "The APC/C subunit Mnd2/Apc15 promotes Cdc20 autoubiquitination and spindle assembly checkpoint inactivation." Mol Cell **47**(6): 921-932.
Frye, J. J., N. G. Brown, G. Petzold, E. R. Watson, C. R. Grace, A. Nourse, M. A. Jarvis, R. W. Kriwacki, J. M. Peters, H. Stark and B. A. Schulman (2013). "Electron microscopy structure of human APC/C(CDH1)-EMI1 reveals multimodal mechanism of E3 ligase shutdown." Nat Struct Mol Biol **20**(7): 827-835.
Fujimitsu, K., M. Grimaldi and H. Yamano (2016). "Cyclin-dependent kinase 1-dependent activation of APC/C ubiquitin ligase." Science **352**(6289): 1121-1124.
Garnett, M. J., J. Mansfeld, C. Godwin, T. Matsusaka, J. Wu, P. Russell, J. Pines and A. R. Venkitaraman (2009). "UBE2S elongates ubiquitin chains on APC/C substrates to promote mitotic exit." Nat Cell Biol **11**(11): 1363-1369.
Girard, J. R., J. L. Tenthorey and D. O. Morgan (2015). "An E2 accessory domain increases affinity for the anaphase-promoting complex and ensures E2 competition." J Biol Chem **290**(40): 24614-24625.
Goddard, T. D., C. C. Huang, E. C. Meng, E. F. Pettersen, G. S. Couch, J. H. Morris and T. E. Ferrin (2018). "UCSF ChimeraX: Meeting modern challenges in visualization and analysis." Protein Sci **27**(1): 14-25.
Golan, A., Y. Yudkovsky and A. Hershko (2002). "The cyclin-ubiquitin ligase activity of cyclosome/APC is jointly activated by protein kinases Cdk1-cyclin B and Plk." J Biol Chem **277**(18): 15552-15557.
Hall, M. C., M. P. Torres, G. K. Schroeder and C. H. Borchers (2003). "Mnd2 and Swm1 are core subunits of the Saccharomyces cerevisiae anaphase-promoting complex." J Biol Chem **278**(19): 16698-16705.
Hall, M. C., E. N. Warren and C. H. Borchers (2004). "Multi-kinase phosphorylation of the APC/C activator Cdh1 revealed by mass spectrometry." Cell Cycle **3**(10): 1278-1284.
Hartooni, N., J. Sung, A. Jain and D. O. Morgan (2022). "Single-molecule analysis of specificity and multivalency in binding of short linear substrate motifs to the APC/C." Nat Commun **13**(1): 341.

He, J., W. C. Chao, Z. Zhang, J. Yang, N. Cronin and D. Barford (2013). "Insights into Degron Recognition by APC/C Coactivators from the Structure of an Acm1-Cdh1 Complex." Mol Cell **50**(5): 649-660.
Hilioti, Z., Y. S. Chung, Y. Mochizuki, C. F. Hardy and O. Cohen-Fix (2001). "The anaphase inhibitor Pds1 binds to the APC/C-associated protein Cdc20 in a destruction box-dependent manner." Curr Biol **11**(17): 1347-1352.
Hockner, S., L. Neumann-Arnold and W. Seufert (2016). "Dual control by Cdk1 phosphorylation of the budding yeast APC/C ubiquitin ligase activator Cdh1." Mol Biol Cell **27**(14): 2198-2212.
Höfler, A., J. Yu, J. Yang, Z. Zhang, L. Chang, S. H. McLaughlin, G. W. Grime, E. F. Garman, A. Boland and D. Barford (2024). "New structural features of the APC/C from high-resolution cryo-EM structures of apo-APC/C and APC/CCDH1:EMI1 complexes." BioRxiv **2023.08.31.555674**.
Jin, L., A. Williamson, S. Banerjee, I. Philipp and M. Rape (2008). "Mechanism of ubiquitin-chain formation by the human anaphase-promoting complex." Cell **133**(4): 653-665.
Jumper, J., R. Evans, A. Pritzel, T. Green, M. Figurnov, O. Ronneberger, K. Tunyasuvunakool, R. Bates, A. Zidek, A. Potapenko, A. Bridgland, C. Meyer, S. A. A. Kohl, A. J. Ballard, A. Cowie, B. Romera-Paredes, S. Nikolov, R. Jain, J. Adler, T. Back, S. Petersen, D. Reiman, E. Clancy, M. Zielinski, M. Steinegger, M. Pacholska, T. Berghammer, S. Bodenstein, D. Silver, O. Vinyals, A. W. Senior, K. Kavukcuoglu, P. Kohli and D. Hassabis (2021). "Highly accurate protein structure prediction with AlphaFold." Nature.
Keller, A., A. I. Nesvizhskii, E. Kolker and R. Aebersold (2002). "Empirical statistical model to estimate the accuracy of peptide identifications made by MS/MS and database search." Anal Chem **74**(20): 5383-5392.
Kimata, Y., J. E. Baxter, A. M. Fry and H. Yamano (2008). "A role for the Fizzy/Cdc20 family of proteins in activation of the APC/C distinct from substrate recruitment." Mol Cell **32**(4): 576-583.
King, R. W., J. M. Peters, S. Tugendreich, M. Rolfe, P. Hieter and M. W. Kirschner (1995). "A 20S complex containing CDC27 and CDC16 catalyzes the mitosis-specific conjugation of ubiquitin to cyclin B." Cell **81**(2): 279-288.
Kraft, C., H. C. Vodermaier, S. Maurer-Stroh, F. Eisenhaber and J. M. Peters (2005). "The WD40 propeller domain of Cdh1 functions as a destruction box receptor for APC/C substrates." Mol Cell **18**(5): 543-553.
Kramer, E. R., N. Scheuringer, A. V. Podtelejnikov, M. Mann and J. M. Peters (2000). "Mitotic regulation of the APC activator proteins CDC20 and CDH1." Mol Biol Cell **11**(5): 1555-1569.
Lahav-Baratz, S., V. Sudakin, J. V. Ruderman and A. Hershko (1995). "Reversible phosphorylation controls the activity of cyclosome-associated cyclin-ubiquitin ligase." Proc Natl Acad Sci U S A **92**(20): 9303-9307.
Lamb, J. R., W. A. Michaud, R. S. Sikorski and P. A. Hieter (1994). "Cdc16p, Cdc23p and Cdc27p form a complex essential for mitosis." Embo J **13**(18): 4321-4328.
Li, Q., L. Chang, S. Aibara, J. Yang, Z. Zhang and D. Barford (2016). "WD40 domain of Apc1 is critical for the coactivator-induced allosteric transition that stimulates APC/C catalytic activity." Proc Natl Acad Sci U S A **113**(38): 10547-10552.
Lu, D., J. Y. Hsiao, N. E. Davey, V. A. Van Voorhis, S. A. Foster, C. Tang and D. O. Morgan (2014). "Multiple mechanisms determine the order of APC/C substrate degradation in mitosis." J Cell Biol **207**(1): 23-39.

Mansfeld, J., P. Collin, M. O. Collins, J. S. Choudhary and J. Pines (2011). "APC15 drives the turnover of MCC-CDC20 to make the spindle assembly checkpoint responsive to kinetochore attachment." Nat Cell Biol **13**(10): 1234-1243.
Martinez, J. S., D. E. Jeong, E. Choi, B. M. Billings and M. C. Hall (2006). "Acm1 is a negative regulator of the CDH1-dependent anaphase-promoting complex/cyclosome in budding yeast." Mol Cell Biol **26**(24): 9162-9176.
Matsumoto, M. L., K. E. Wickliffe, K. C. Dong, C. Yu, I. Bosanac, D. Bustos, L. Phu, D. S. Kirkpatrick, S. G. Hymowitz, M. Rape, R. F. Kelley and V. M. Dixit (2010). "K11-linked polyubiquitination in cell cycle control revealed by a K11 linkage-specific antibody." Mol Cell **39**(3): 477-484.
Matyskiela, M. E. and D. O. Morgan (2009). "Analysis of activator-binding sites on the APC/C supports a cooperative substrate-binding mechanism." Mol Cell **34**(1): 68-80.
Nakane, T., D. Kimanius, E. Lindahl and S. H. Scheres (2018). "Characterisation of molecular motions in cryo-EM single-particle data by multi-body refinement in RELION." Elife **7**.
Ng, H. Y., A. N. Adly, D. H. Whelpley, R. T. Suhandynata, H. Zhou and D. O. Morgan (2024). "Phosphate-binding pocket on cyclin B governs CDK substrate phosphorylation and mitotic timing." bioRxiv.
Oelschlaegel, T., M. Schwickart, J. Matos, A. Bogdanova, A. Camasses, J. Havlis, A. Shevchenko and W. Zachariae (2005). "The yeast APC/C subunit Mnd2 prevents premature sister chromatid separation triggered by the meiosis-specific APC/C-Ama1." Cell **120**(6): 773-788.
Ohi, M. D., A. Feoktistova, L. Ren, C. Yip, Y. Cheng, J. S. Chen, H. J. Yoon, J. S. Wall, Z. Huang, P. A. Penczek, K. L. Gould and T. Walz (2007). "Structural organization of the anaphase-promoting complex bound to the mitotic activator Slp1." Mol Cell **28**(5): 871-885.
Passmore, L. A., D. Barford and J. W. Harper (2005). "Purification and assay of the budding yeast anaphase-promoting complex." Methods Enzymol **398**: 195-219.
Passmore, L. A., E. A. McCormack, S. W. Au, A. Paul, K. R. Willison, J. W. Harper and D. Barford (2003). "Doc1 mediates the activity of the anaphase-promoting complex by contributing to substrate recognition." Embo J **22**(4): 786-796.
Penkner, A. M., S. Prinz, S. Ferscha and F. Klein (2005). "Mnd2, an essential antagonist of the anaphase-promoting complex during meiotic prophase." Cell **120**(6): 789-801.
Perkins, D. N., D. J. Pappin, D. M. Creasy and J. S. Cottrell (1999). "Probability-based protein identification by searching sequence databases using mass spectrometry data." Electrophoresis **20**(18): 3551-3567.
Qiao, R., F. Weissmann, M. Yamaguchi, N. G. Brown, R. VanderLinden, R. Imre, M. A. Jarvis, M. R. Brunner, I. F. Davidson, G. Litos, D. Haselbach, K. Mechtler, H. Stark, B. A. Schulman and J. M. Peters (2016). "Mechanism of APC/CCDC20 activation by mitotic phosphorylation." Proc Natl Acad Sci U S A **113**(19): E2570-2578.
Reimann, J. D., E. Freed, J. Y. Hsu, E. R. Kramer, J. M. Peters and P. K. Jackson (2001). "Emi1 is a mitotic regulator that interacts with Cdc20 and inhibits the anaphase promoting complex." Cell **105**(5): 645-655.
Reimann, J. D., B. E. Gardner, F. Margottin-Goguet and P. K. Jackson (2001). "Emi1 regulates the anaphase-promoting complex by a different mechanism than Mad2 proteins." Genes Dev **15**(24): 3278-3285.
Rodrigo-Brenni, M. C., S. A. Foster and D. O. Morgan (2010). "Catalysis of lysine 48-specific ubiquitin chain assembly by residues in E2 and ubiquitin." Mol Cell **39**(4): 548-559.

Rodrigo-Brenni, M. C. and D. O. Morgan (2007). "Sequential E2s drive polyubiquitin chain assembly on APC targets." Cell **130**(1): 127-139.
Rudner, A. D. and A. W. Murray (2000). "Phosphorylation by Cdc28 activates the Cdc20-dependent activity of the anaphase-promoting complex." J Cell Biol **149**(7): 1377-1390.
Schreiber, A., F. Stengel, Z. Zhang, R. I. Enchev, E. H. Kong, E. P. Morris, C. V. Robinson, P. C. da Fonseca and D. Barford (2011). "Structural basis for the subunit assembly of the anaphase-promoting complex." Nature **470**(7333): 227-232.
Schwab, M., M. Neutzner, D. Mocker and W. Seufert (2001). "Yeast Hct1 recognizes the mitotic cyclin Clb2 and other substrates of the ubiquitin ligase APC." Embo J **20**(18): 5165-5175.
Schwickart, M., J. Havlis, B. Habermann, A. Bogdanova, A. Camasses, T. Oelschlaegel, A. Shevchenko and W. Zachariae (2004). "Swm1/Apc13 is an evolutionarily conserved subunit of the anaphase-promoting complex stabilizing the association of Cdc16 and Cdc27." Mol Cell Biol **24**(8): 3562-3576.
Shteinberg, M., Y. Protopopov, T. Listovsky, M. Brandeis and A. Hershko (1999). "Phosphorylation of the cyclosome is required for its stimulation by Fizzy/cdc20." Biochem Biophys Res Commun **260**(1): 193-198.
Sikorski, R. S., M. S. Boguski, M. Goebl and P. Hieter (1990). "A repeating amino acid motif in CDC23 defines a family of proteins and a new relationship among genes required for mitosis and RNA synthesis." Cell **60**(2): 307-317.
Sikorski, R. S., W. A. Michaud, J. C. Wootton, M. S. Boguski, C. Connelly and P. Hieter (1991). "TPR proteins as essential components of the yeast cell cycle." Cold Spring Harb Symp Quant Biol **56**: 663-673.
Sudakin, V., G. K. Chan and T. J. Yen (2001). "Checkpoint inhibition of the APC/C in HeLa cells is mediated by a complex of BUBR1, BUB3, CDC20, and MAD2." J Cell Biol **154**(5): 925-936.
Tian, W., B. Li, R. Warrington, D. R. Tomchick, H. Yu and X. Luo (2012). "Structural analysis of human Cdc20 supports multisite degron recognition by APC/C." Proc Natl Acad Sci U S A **109**(45): 18419-18424.
Torres, M. P. and C. H. Borchers (2007). "Mitotic phosphorylation of the anaphase-promoting complex inhibitory subunit Mnd2 is necessary for efficient progression through meiosis i." J Biol Chem **282**(24): 17351-17362.
Tunyasuvunakool, K., J. Adler, Z. Wu, T. Green, M. Zielinski, A. Zidek, A. Bridgland, A. Cowie, C. Meyer, A. Laydon, S. Velankar, G. J. Kleywegt, A. Bateman, R. Evans, A. Pritzel, M. Figurnov, O. Ronneberger, R. Bates, S. A. A. Kohl, A. Potapenko, A. J. Ballard, B. Romera-Paredes, S. Nikolov, R. Jain, E. Clancy, D. Reiman, S. Petersen, A. W. Senior, K. Kavukcuoglu, E. Birney, P. Kohli, J. Jumper and D. Hassabis (2021). "Highly accurate protein structure prediction for the human proteome." Nature.
Uzunova, K., B. T. Dye, H. Schutz, R. Ladurner, G. Petzold, Y. Toyoda, M. A. Jarvis, N. G. Brown, I. Poser, M. Novatchkova, K. Mechtler, A. A. Hyman, H. Stark, B. A. Schulman and J. M. Peters (2012). "APC15 mediates CDC20 autoubiquitylation by APC/C(MCC) and disassembly of the mitotic checkpoint complex." Nat Struct Mol Biol **19**(11): 1116-1123.
Van Voorhis, V. A. and D. O. Morgan (2014). "Activation of the APC/C ubiquitin ligase by enhanced E2 efficiency." Curr Biol **24**(13): 1556-1562.
Vodermaier, H. C., C. Gieffers, S. Maurer-Stroh, F. Eisenhaber and J. M. Peters (2003). "TPR subunits of the anaphase-promoting complex mediate binding to the activator protein CDH1." Curr Biol **13**(17): 1459-1468.

Wang, J., B. T. Dye, K. R. Rajashankar, I. Kurinov and B. A. Schulman (2009). "Insights into anaphase promoting complex TPR subdomain assembly from a CDC26-APC6 structure." Nat Struct Mol Biol.
Waterhouse, A. M., J. B. Procter, D. M. Martin, M. Clamp and G. J. Barton (2009). "Jalview Version 2--a multiple sequence alignment editor and analysis workbench." Bioinformatics **25**(9): 1189-1191.
Watson, E. R., N. G. Brown, J. M. Peters, H. Stark and B. A. Schulman (2019). "Posing the APC/C E3 Ubiquitin Ligase to Orchestrate Cell Division." Trends Cell Biol **29**(2): 117-134.
Watson, E. R., C. R. R. Grace, W. Zhang, D. J. Miller, I. F. Davidson, J. R. Prabu, S. Yu, D. L. Bolhuis, E. T. Kulko, R. Vollrath, D. Haselbach, H. Stark, J. M. Peters, N. G. Brown, S. S. Sidhu and B. A. Schulman (2019). "Protein engineering of a ubiquitin-variant inhibitor of APC/C identifies a cryptic K48 ubiquitin chain binding site." Proc Natl Acad Sci U S A.
Wendt, K. S., H. C. Vodermaier, U. Jacob, C. Gieffers, M. Gmachl, J. M. Peters, R. Huber and P. Sondermann (2001). "Crystal structure of the APC10/DOC1 subunit of the human anaphase-promoting complex." Nat Struct Biol **8**(9): 784-788.
Wickliffe, K. E., S. Lorenz, D. E. Wemmer, J. Kuriyan and M. Rape (2011). "The mechanism of linkage-specific ubiquitin chain elongation by a single-subunit e2." Cell **144**(5): 769-781.
Williams, C. J., J. J. Headd, N. W. Moriarty, M. G. Prisant, L. L. Videau, L. N. Deis, V. Verma, D. A. Keedy, B. J. Hintze, V. B. Chen, S. Jain, S. M. Lewis, W. B. Arendall, 3rd, J. Snoeyink, P. D. Adams, S. C. Lovell, J. S. Richardson and D. C. Richardson (2018). "MolProbity: More and better reference data for improved all-atom structure validation." Protein Sci **27**(1): 293-315.
Williamson, A., K. E. Wickliffe, B. G. Mellone, L. Song, G. H. Karpen and M. Rape (2009). "Identification of a physiological E2 module for the human anaphase-promoting complex." Proc Natl Acad Sci U S A **106**(43): 18213-18218.
Yamaguchi, M., R. VanderLinden, F. Weissmann, R. P. Qiao, P. Dube, N. G. Brown, D. Haselbach, W. Zhang, S. S. Sidhu, J. M. Peters, H. Stark and B. A. Schulman (2016). "Cryo-EM of Mitotic Checkpoint Complex-Bound APC/C Reveals Reciprocal and Conformational Regulation of Ubiquitin Ligation." Molecular Cell **63**(4): 593-607.
Yang, Z., K. Lasker, D. Schneidman-Duhovny, B. Webb, C. C. Huang, E. F. Pettersen, T. D. Goddard, E. C. Meng, A. Sali and T. E. Ferrin (2012). "UCSF Chimera, MODELLER, and IMP: an integrated modeling system." J Struct Biol **179**(3): 269-278.
Yatskevich, S., J. S. Kroonen, C. Alfieri, T. Tischer, A. C. Howes, L. Clijsters, J. Yang, Z. Zhang, K. Yan, A. C. O. Vertegaal and D. Barford (2021). "Molecular mechanisms of APC/C release from spindle assembly checkpoint inhibition by APC/C SUMOylation." Cell Rep **34**(13): 108929.
Zachariae, W., M. Schwab, K. Nasmyth and W. Seufert (1998). "Control of cyclin ubiquitination by CDK-regulated binding of Hct1 to the anaphase promoting complex." Science **282**(5394): 1721-1724.
Zachariae, W., A. Shevchenko, P. D. Andrews, R. Ciosk, M. Galova, M. J. Stark, M. Mann and K. Nasmyth (1998). "Mass spectrometric analysis of the anaphase-promoting complex from yeast: identification of a subunit related to cullins." Science **279**(5354): 1216-1219.
Zachariae, W., T. H. Shin, M. Galova, B. Obermaier and K. Nasmyth (1996). "Identification of subunits of the anaphase-promoting complex of Saccharomyces cerevisiae." Science **274**(5290): 1201-1204.
Zhang, K. (2016). "Gctf: Real-time CTF determination and correction." J Struct Biol **193**(1): 1-12.

Zhang, S., L. Chang, C. Alfieri, Z. Zhang, J. Yang, S. Maslen, M. Skehel and D. Barford (2016). "Molecular mechanism of APC/C activation by mitotic phosphorylation." Nature **533**(7602): 260-264.
Zhang, S., T. Tischer and D. Barford (2019). "Cyclin A2 degradation during the spindle assembly checkpoint requires multiple binding modes to the APC/C." Nat Commun **10**(1): 3863.
Zhang, Z., L. Chang, J. Yang, N. Conin, K. Kulkarni and D. Barford (2013). "The four canonical tpr subunits of human APC/C form related homo-dimeric structures and stack in parallel to form a TPR suprahelix." J Mol Biol **425**(22): 4236-4248.
Zhang, Z., K. Kulkarni, S. J. Hanrahan, A. J. Thompson and D. Barford (2010). "The APC/C subunit Cdc16/Cut9 is a contiguous tetratricopeptide repeat superhelix with a homo-dimer interface similar to Cdc27." EMBO J **29**(21): 3733-3744.
Zhang, Z., S. M. Roe, M. Diogon, E. Kong, H. El Alaoui and D. Barford (2010). "Molecular structure of the N-terminal domain of the APC/C subunit Cdc27 reveals a homo-dimeric tetratricopeptide repeat architecture." J Mol Biol **397**(5): 1316-1328.
Zhang, Z., J. Yang and D. Barford (2016). "Recombinant expression and reconstitution of multiprotein complexes by the USER cloning method in the insect cell-baculovirus expression system." Methods **95**: 13-25.
Zhang, Z., J. Yang, E. H. Kong, W. C. Chao, E. P. Morris, P. C. da Fonseca and D. Barford (2013). "Recombinant expression, reconstitution and structure of human anaphase-promoting complex (APC/C)." Biochem J **449**(2): 365-371.
Zheng, S. Q., E. Palovcak, J. P. Armache, K. A. Verba, Y. Cheng and D. A. Agard (2017). "MotionCor2: anisotropic correction of beam-induced motion for improved cryo-electron microscopy." Nat Methods **14**(4): 331-332.
Zivanov, J., T. Nakane, B. O. Forsberg, D. Kimanius, W. J. Hagen, E. Lindahl and S. H. Scheres (2018). "New tools for automated high-resolution cryo-EM structure determination in RELION-3." Elife **7**.

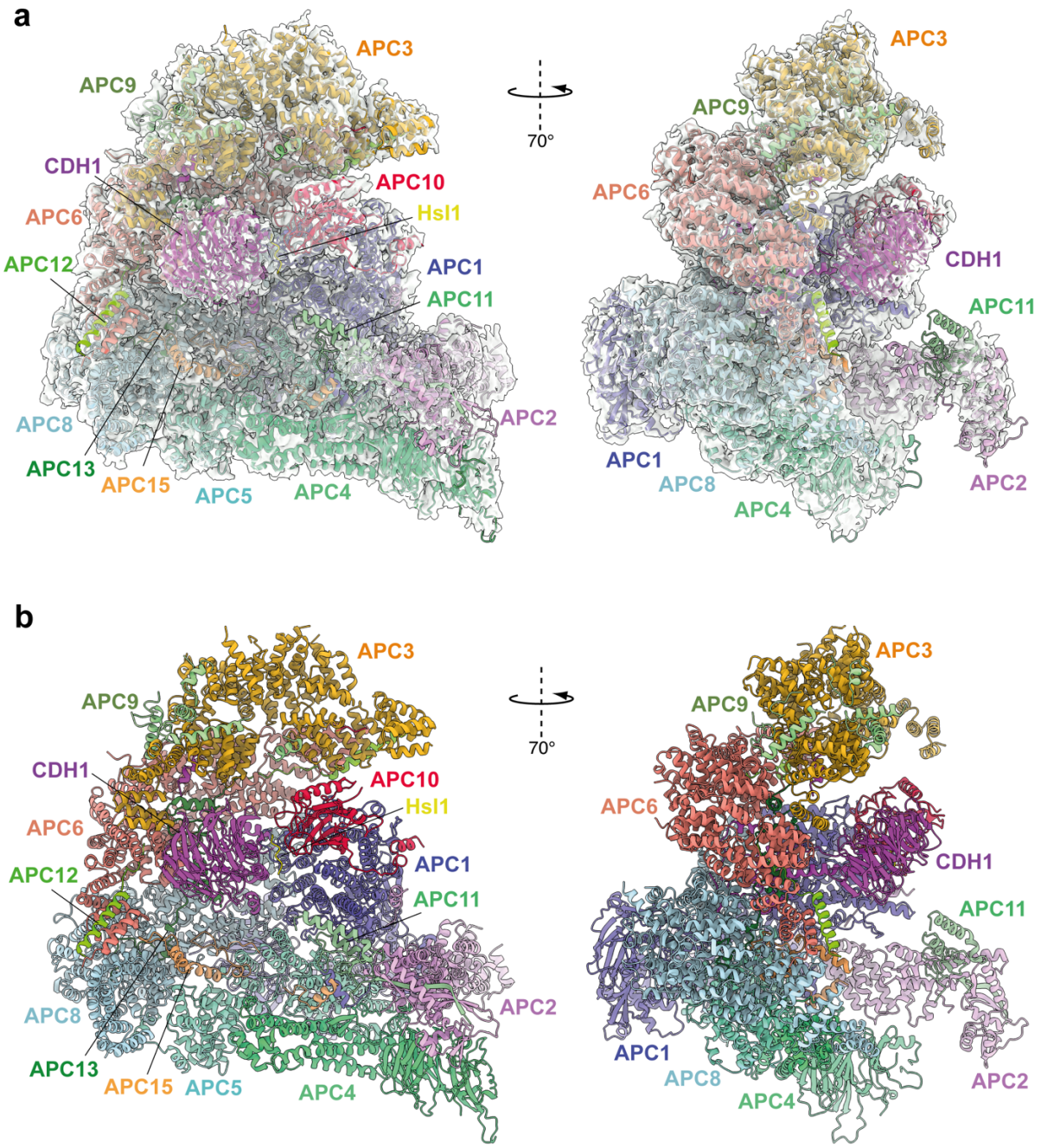

Figure 1. Overall structure of the APC/C$^{CDH1:Hsl1}$ complex. a, Two views of the APC/C$^{CDH1:Hsl1}$ ternary complex fitted into the 4.0 Å cryo-EM map. **b**, Two views of the APC/C$^{CDH1:Hsl1}$ ternary complex shown as ribbon representations.

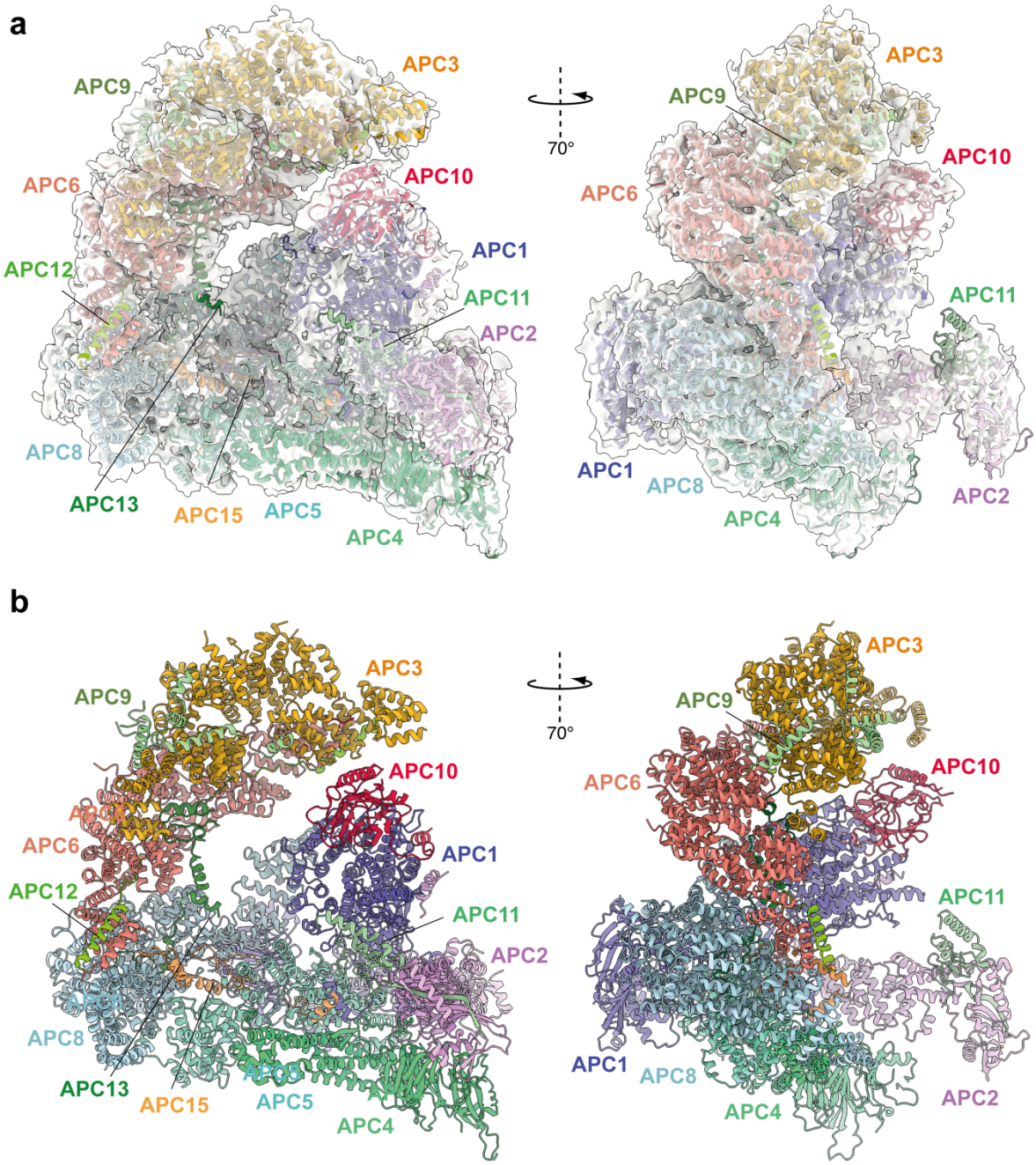

Figure 2. Overall structure of unphosphorylated apo-APC/C. a, Two views of apo-APC/C fitted into the 4.9 Å cryo-EM map. **b**, Two views of apo-APC/C shown as ribbon representations.

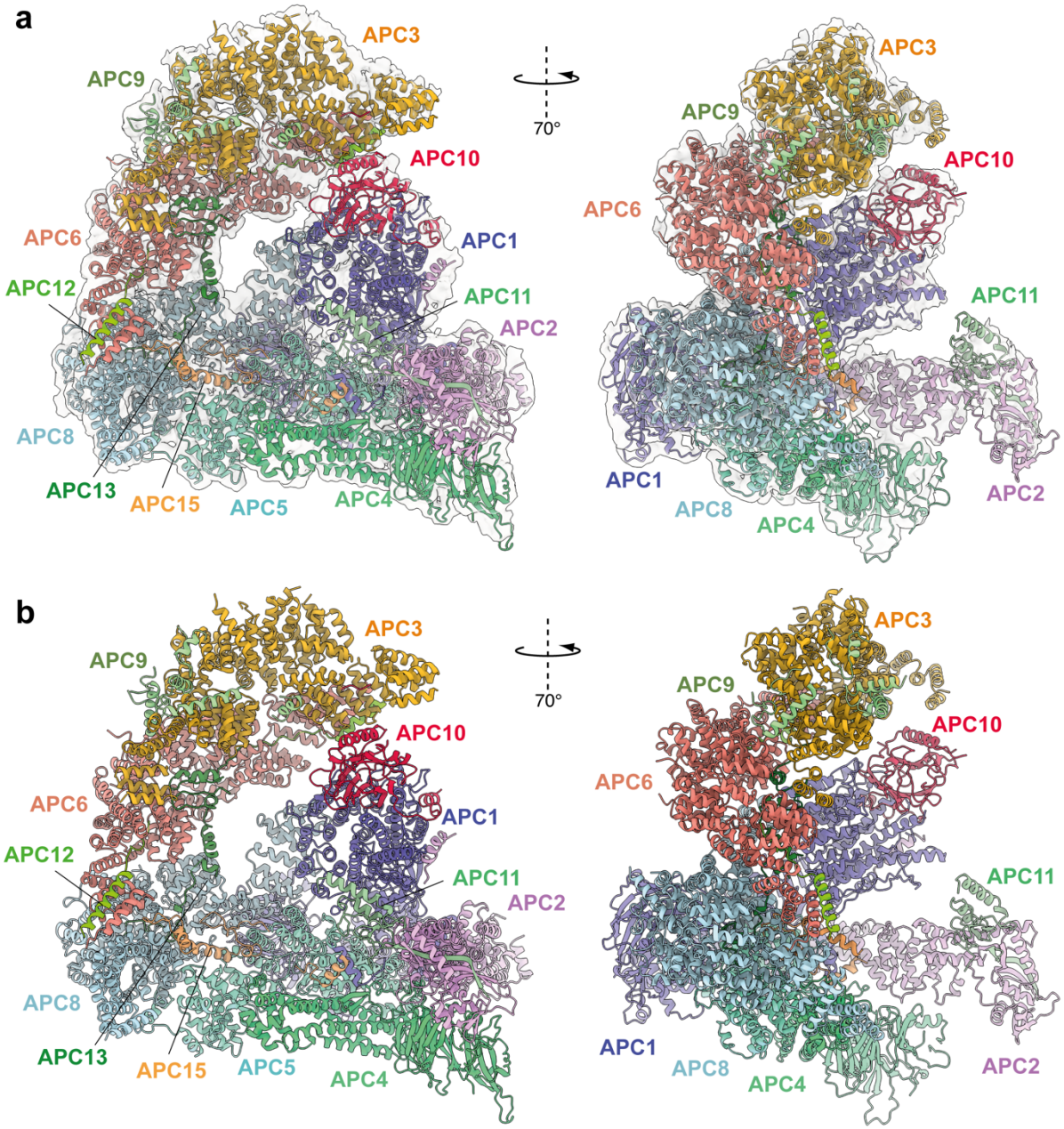

Figure 3. Overall structure of phosphorylated apo-APC/C. a, Two views of phosphorylated apo-APC/C fitted into the 4.5 Å cryo-EM map. **b**, Two views of apo-APC/C shown as ribbon representations.

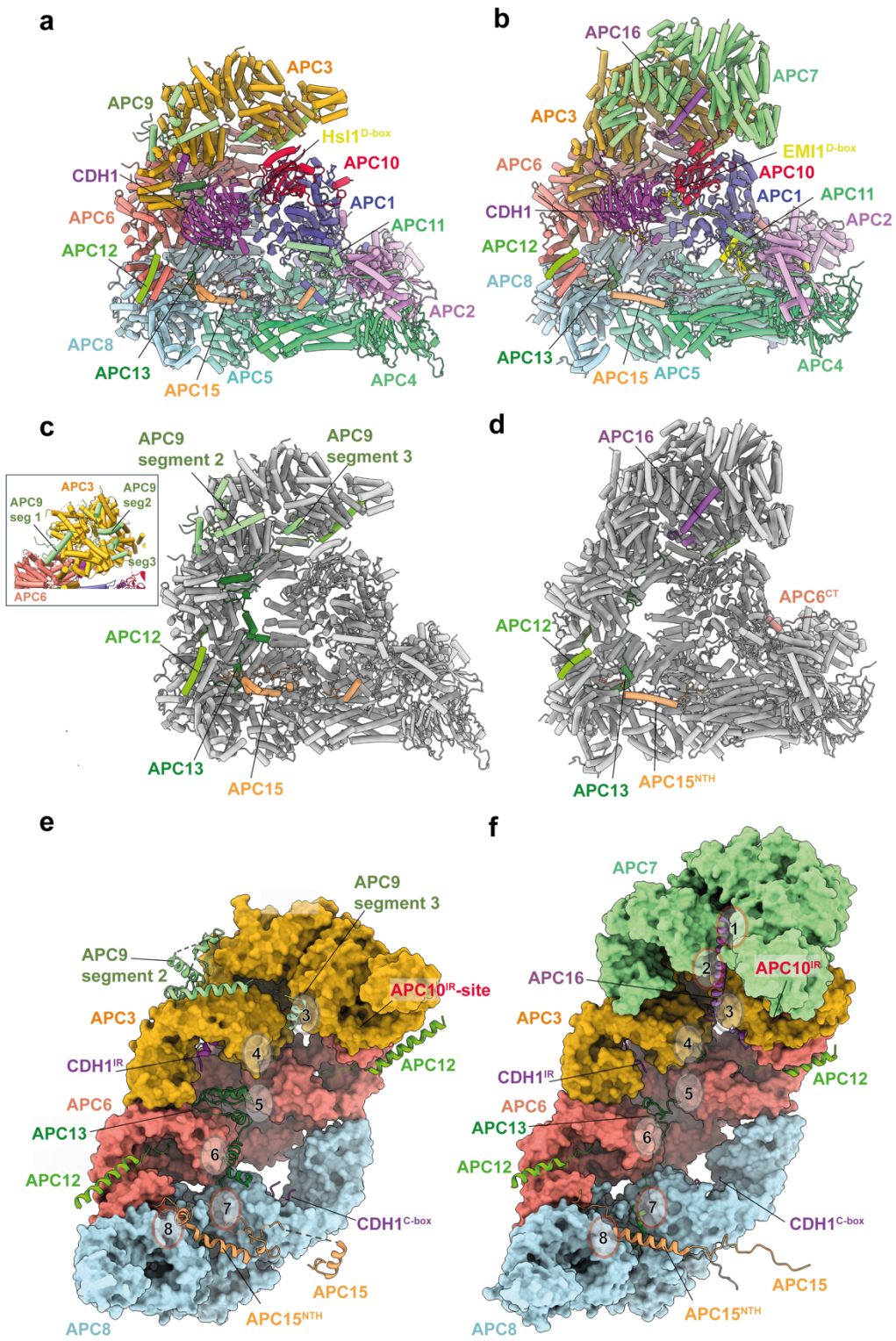

Figure 4. Comparison of *S. cerevisiae* APC/C$^{CDH1:Hsl1}$ with human APC/C$^{CDH1:EMI1}$. a, *S. cerevisiae* and **b,** human complexes subunits colour-coded. **c**, *S. cerevisiae* and **d**, human complexes with large subunits coloured in grey and small IDP subunits (APC9, APC12, APC13, APC15, APC16) colour-coded. The structure of human APC/C$^{CDH1:EMI1}$ from (Höfler, Yu et al. 2024) (PDB 7QE7). **e**, and **f**, Four small IDP-subunits (APC9, APC13, APC15, APC16) contribute to interacting with equivalent, quasi-symmetrical sites on the outer surfaces of the TPR subunits of the TPR lobe. TPR lobes of *S. cerevisiae* (e) and human APC/C (f) are depicted as a surface representations. The contact sites with the three small subunits that contact the *S. cerevisiae* TPR lobe are numbered 3 to 8 after human APC/C (Chang, Zhang et al. 2015) that has sites 8 sites sue to APC7.

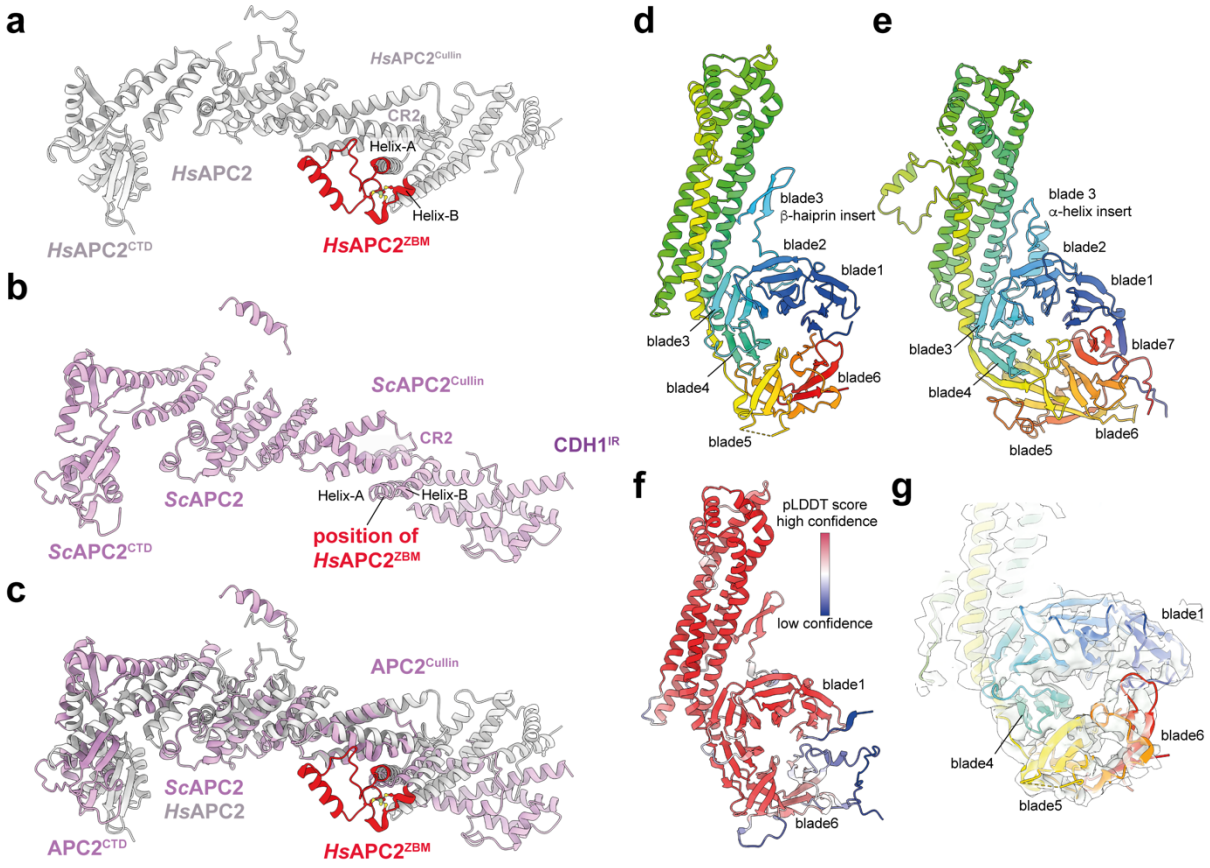

Figure 5. Comparison of *S. cerevisiae* and human APC2 and APC4 subunits. a, Human APC2 with APC2^{ZBM} of CRL2 coloured red. **b**, *S. cerevisiae* APC2. The position of human APC2^{ZBM} is indicated. **c**, Superimposition *S. cerevisiae* APC2 (purple) with human APC2 (grey) on CRL2. Human APC2 from (Höfler, Yu et al. 2024) (PDB 7QE7). **d,** *S. cerevisiae* APC4, colour-coded from N- to C-termini with a blue to red ramp. **e**, Human APC4, colour-coded from N- to C-termini with a blue to red ramp. *S. cerevisiae* APC4^{WD40} is a six-bladed β-propeller in contrast to the seven bladed β-propeller of human APC4^{WD40}. **f**, AlphaFold2 prediction of *S. cerevisiae* APC4 colour-coded according to pLDDT score. No seventh bade is predicted. The α-helix in place of the seventh blade is predicted with low confidence. **g**, Fit of *S. cerevisiae* APC4^{WD40} into the APC/C$^{CDH1:Hsl1}$ cryo-EM map showing lack of density for a seventh blade. Human APC4 from (Höfler, Yu et al. 2024) (PDB 7QE7).

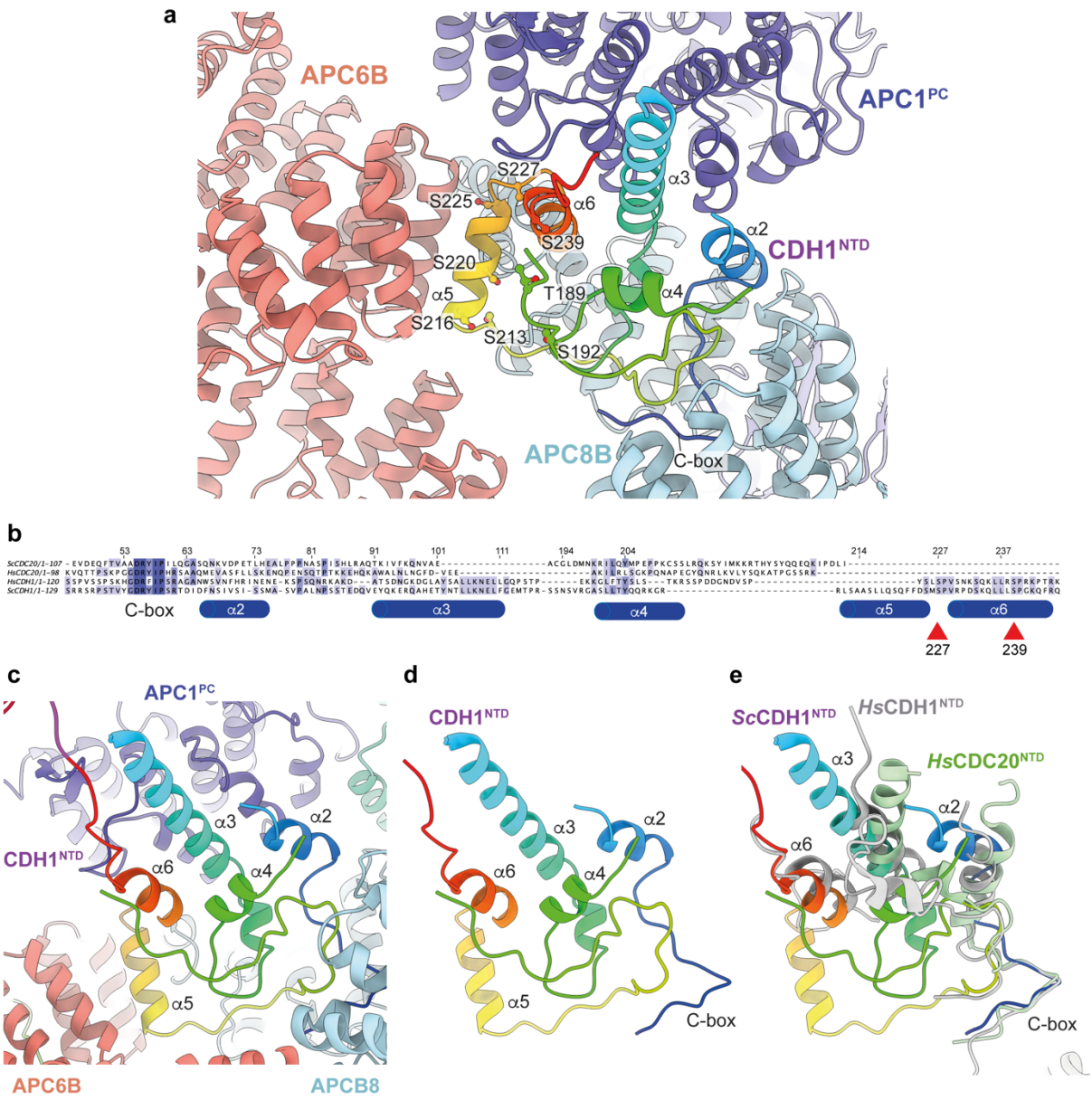

Figure 6. **CDH1^{NTD} contacts to APC/C and control by phosphorylation. a**, In *S. cerevisiae* CDH1, α2, α3 and α6 contact the PC domain of APC1 (APC1^{PC}) (conserved with human CDH1). α2 also contacts APC8B. α5, unique to *S. cerevisiae* CDH1, forms extensive contacts to APC6B. Human CDC20^{NTD} (light green) shares α2 and α3 with CDH1^{NTD}. **b**, MSA of *S. cerevisiae* and human CDH1^{NTD} and CDC20^{NTD} showing α-helices α2 to α6 of *S. cerevisiae* CDH1^{NTD} and the conserved sites of CDK phosphorylation on CDH1 (red arrows). **c**, *S. cerevisiae* CDH1^{NTD} colour-coded from N- to C-termini with a blue to red ramp interacting with APC1^{PC}, APC6B and APC8B. **d**, Same view as (c) without APC1^{PC}, APC6B and APC8B. **e**, Superimposition of *S. cerevisiae* CDH1^{NTD} coloured blue-to-red, human CDH1^{NTD} (grey) (from (Höfler, Yu et al. 2024), PDB 7QE7) and human CDC20^{NTD} (light green) (from (Zhang, Tischer et al. 2019) PDB 6Q6G). α-helices α2, α3 and α6 are conserved in all three structures.

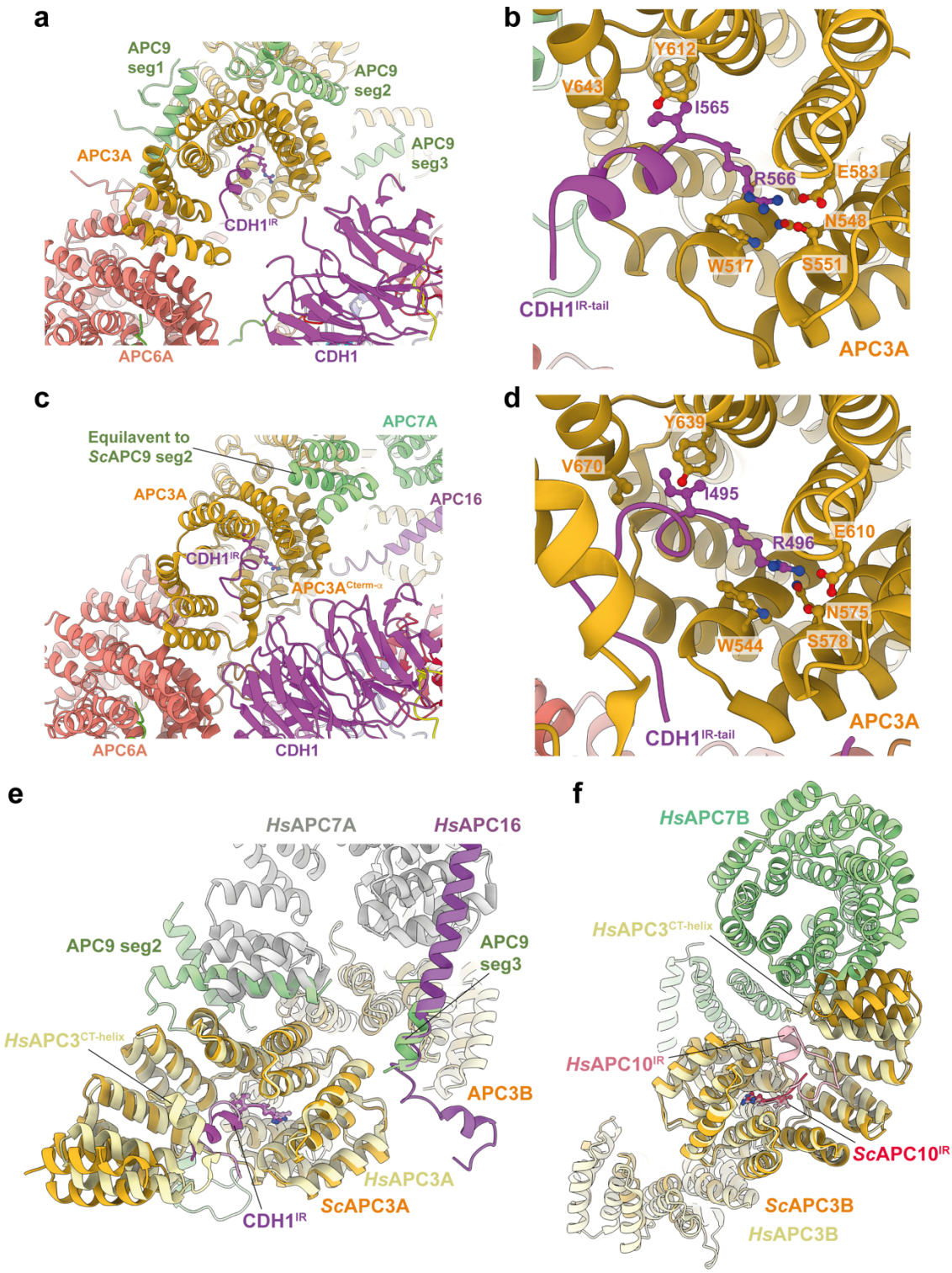

Figure 7. Comparison of CDH1^{IR} binding to *S. cerevisiae* and human APC/C^{CDH1} complexes. a, Overall view of the CDH1^{IR}-binding site on *S. cerevisiae* APC/C$^{CDH1:Hsl1}$. **b**, Zoomed view of this complex. **c,** Overall view of the CDH1^{IR}-binding site on human APC/C$^{CDH1:EMI1}$. **d**, Zoomed view of this complex. The structure of human APC/C$^{CDH1:EMI1}$ from (Höfler, Yu et al. 2024) (PDB 7QE7). **e, f,** APC9 of *S. cerevisiae* APC/C partially mimics APC7 and APC16 of human APC/C. (e) In *S. cerevisiae* APC/C, the interaction of APC9 with APC3A (segment 2 of APC9) and APC3B (segment 3 of APC9) partially mimics the respective APC7 and APC16 interactions with human APC3. APC9 segment 2 interactions with the C-terminal TPR helix of APC3A may stabilise the CDH1^{IR}-binding site of APC3A. **f**, Similarly, in human APC/C, the interface of APC7B with APC3B might function to stabilise the APC10^{IR}-binding site on APC3B. Human APC/C$^{CDH1:EMI1}$ from (Höfler, Yu et al. 2024) (PDB 7QE7).

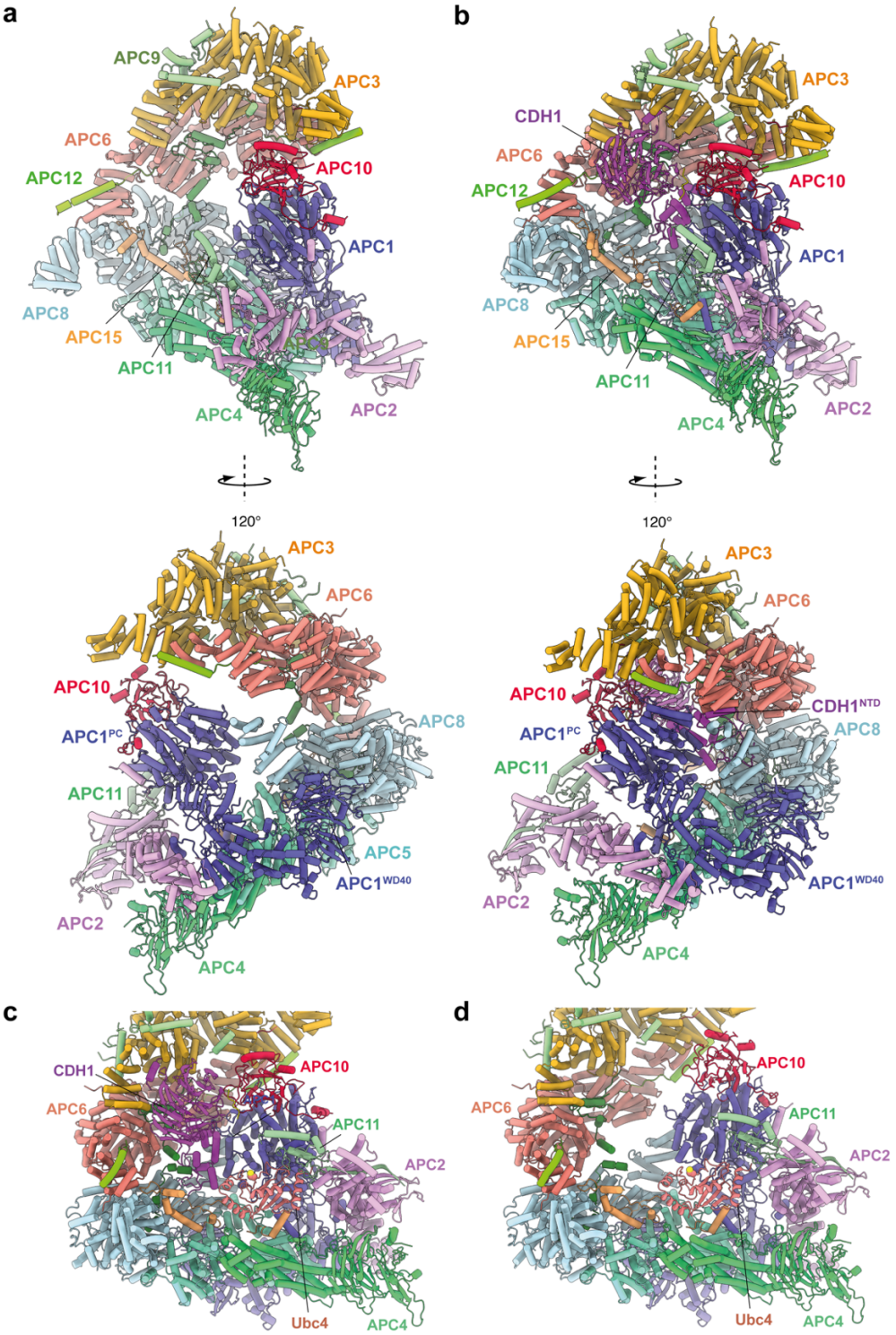

Figure 8. Comparing apo-APC/C and the APC/C$^{CDH1:Hsl1}$ complex shows both apo-APC/C and the APC/C$^{CDH1:Hsl1}$ complexes are competent to bind the Ubc4. **a,** Two views of apo-APC/C. **b**, Two views of APC/C$^{CDH1:Hsl1}$. The coordinates were superimposed on APC1^{PC}. In the apo-APC/C complex, there are no contacts between APC1^{PC} of the platform module and APC6B and APC8B of the TPR lobe. In the APC/C$^{CDH1:Hsl1}$, CDH1^{NTD} bridges APC1^{PC} with APC6B and APC8B. The overall conformations are similar, specifically the APC2:APC11 catalytic module adopts a raised conformation in both states. **c**, Model of APC/C$^{CDH1:Hsl1}$ in complex with Ubc4. **d**, Model of apo-APC/C in complex with Ubc4. The position of the APC2:APC11 catalytic module in apo-APC/C does not exclude Ubc4

binding (d). Model of APC11:E2 based on the *S. cerevisiae* Not4 RING:Ubc4 complex (PDB 5AIE) (Bhaskar, Basquin et al. 2015).

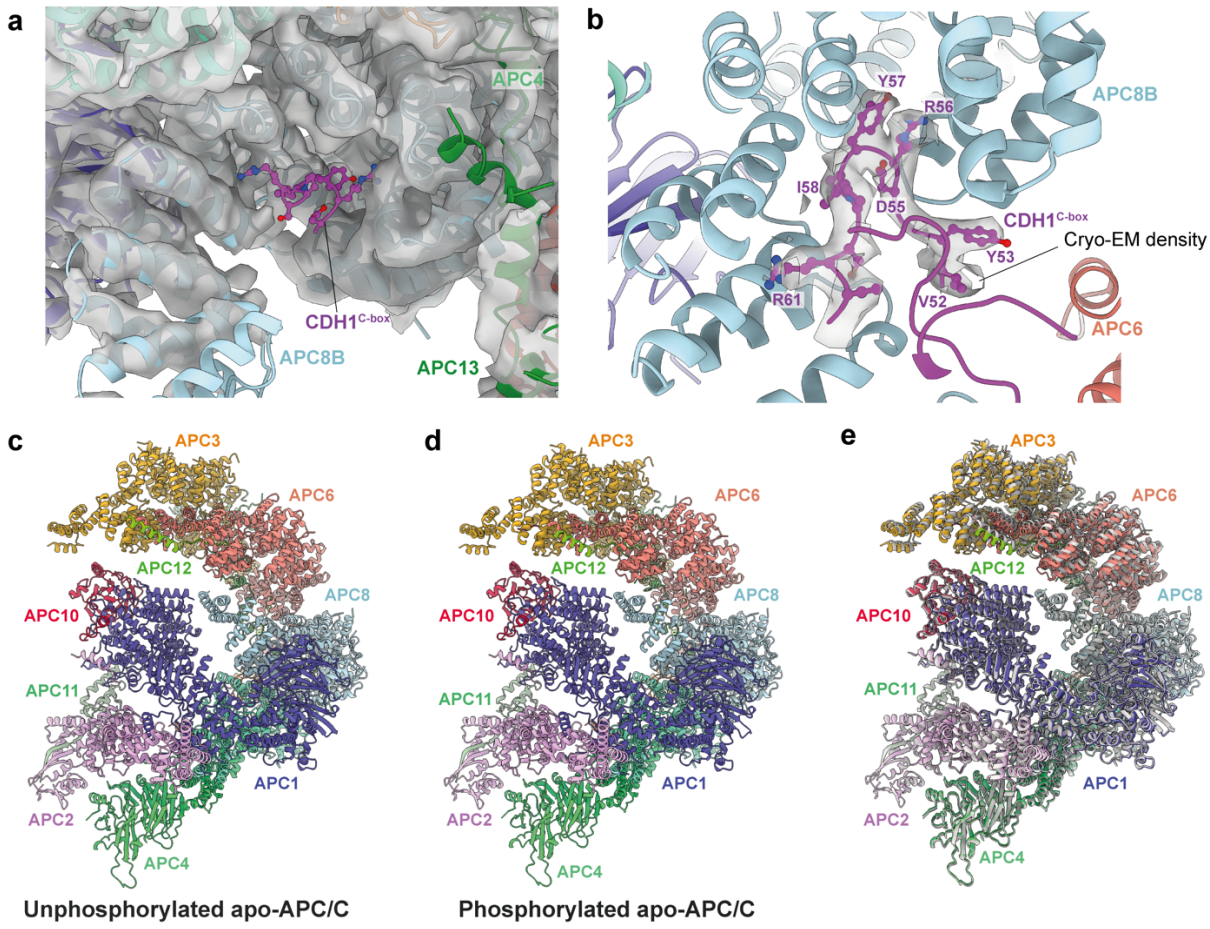

Figure 9. Regulation of APC/C by phosphorylation. The C-box binding site is un-obstructed in unphosphorylated apo-APC/C. a, Cryo-EM density from the unphosphorylated apo-APC/C map corresponding to the C-box binding site of APC8B with the fitted $CDH1^{C\text{-}box}$ modelled from $APC/C^{CDH1:Hsl1}$. We observe no density at the APC8B C-box binding site. **b**, Cryo-EM map density for the $CDH1^{C\text{-}box}$ from the $APC/C^{CDH1:Hsl1}$ reconstruction with fitted coordinates. **c-e**, Comparison of unphosphorylated apo-APC/C and phosphorylated apo-APC/C**:** (c) Unphosphorylated apo-APC/C. (d) Phosphorylated apo-APC/C. (e) Superimposition of unphosphorylated apo-APC/C (coloured by subunit assignment) and phosphorylated apo-APC/C (grey). There is a small relative shift of the TPR lobe. The coordinates were superimposed on $APC1^{PC}$.

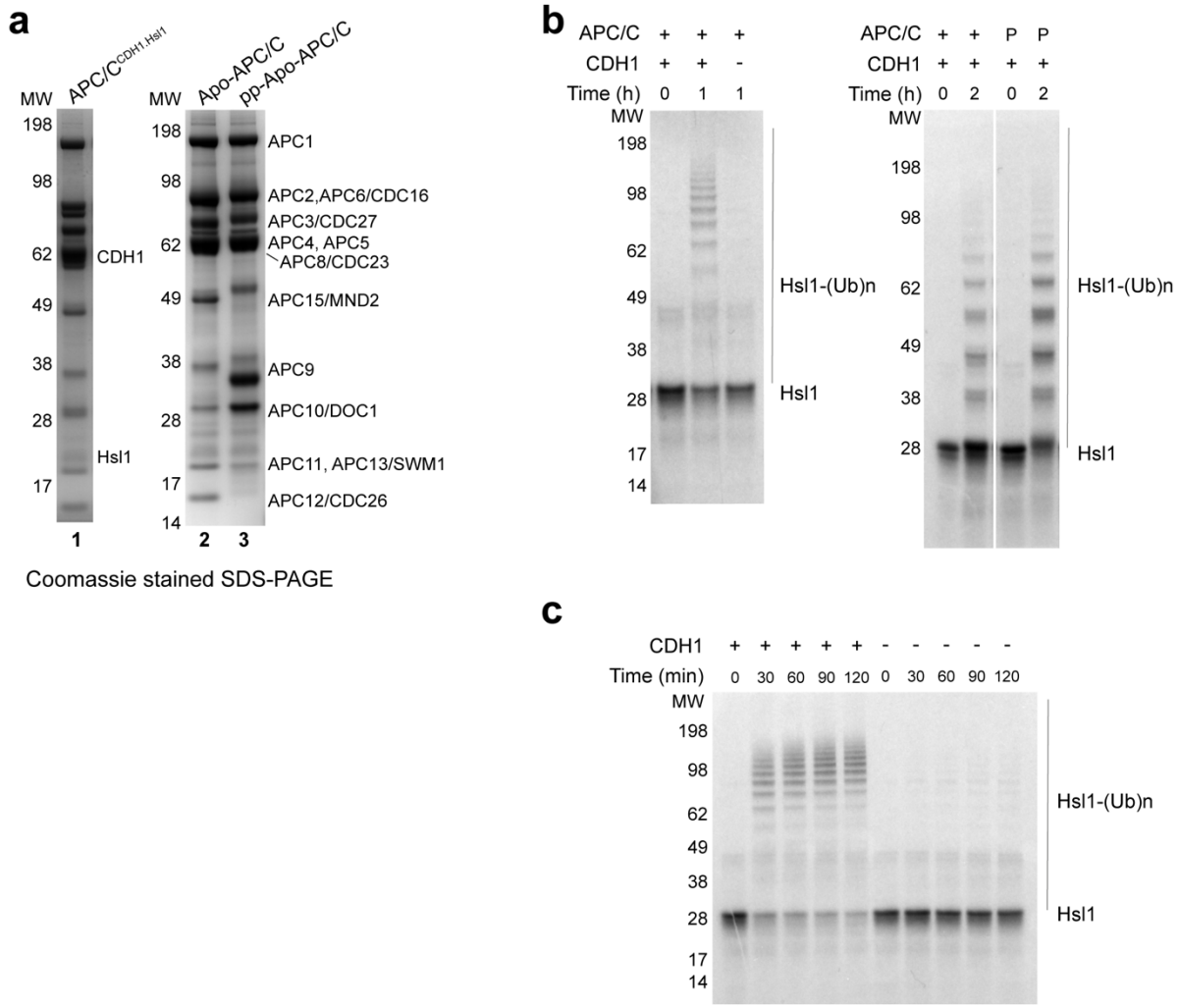

Supplementary Figure 1. SDS PAGE gels of purified APC/C complexes and ubiquitylation assays. **a**, APC/C$^{CDH1:Hsl1}$ complex, unphosphorylated apo-APC, phosphorylated apo-APC (lanes 1-3). **b**, Ubiquitylation assay showing activation by CDH1. Phosphorylation (P: phosphorylated APC/C) did not significantly affect activity. **c,** Time course of ubiquitylation reaction**.**

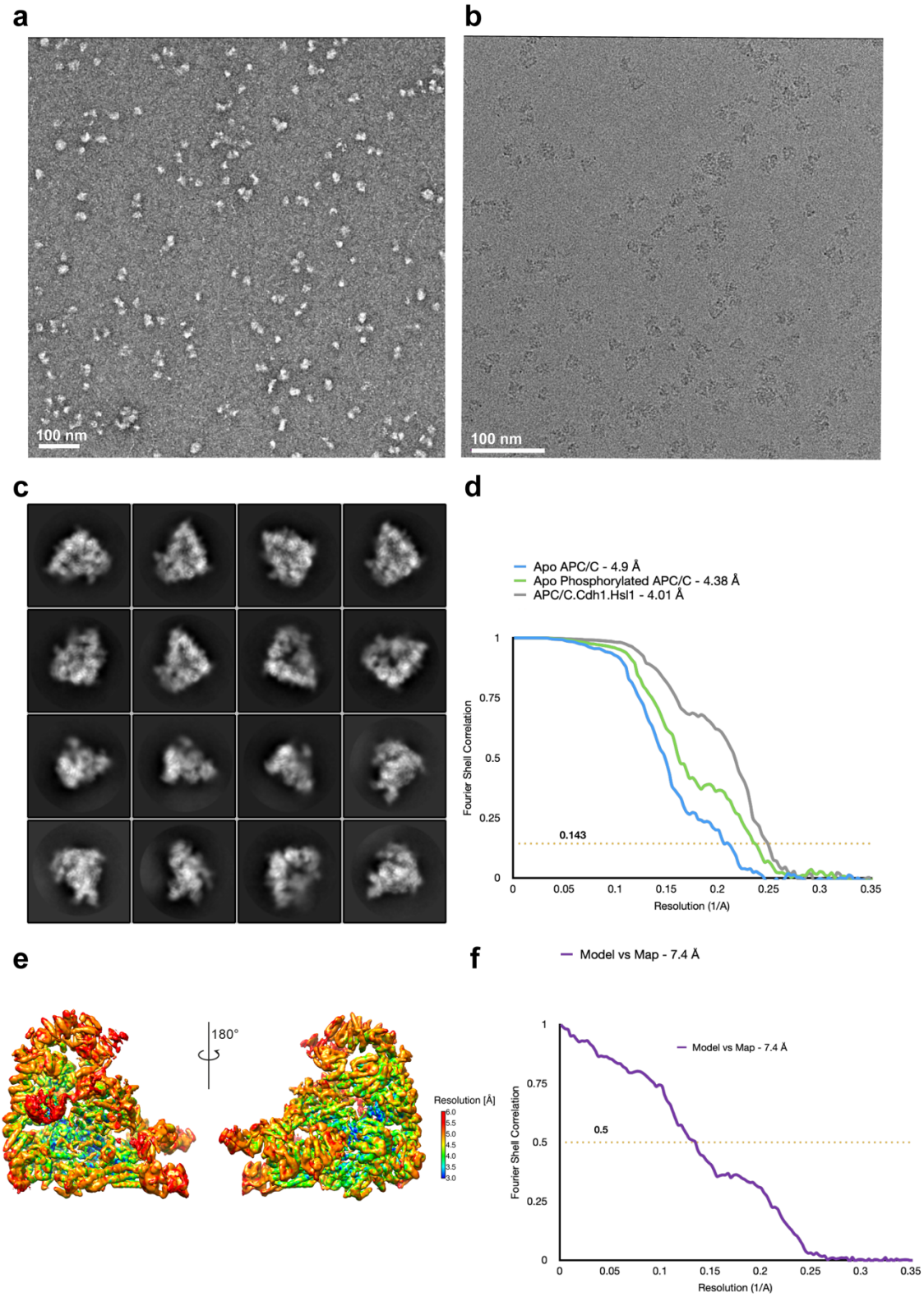

Supplementary Figure 2. EM images and 2D class averages of APC/C$^{CDH1:Hsl1}$ complex. a, Representative negative stain image of the APC/C$^{CDH1:Hsl1}$ complex. **b,** Representative cryo-EM image of the APC/C$^{CDH1:Hsl1}$ complex. **c**, Gallery of 2D-class averages of APC/C$^{CDH1:Hsl1}$. **d**, Fourier Shell Correlation (FSC) plots of the main maps used to generate molecular models APC/C$^{CDH1:Hsl1}$, unphosphorylated apo-APC/C and phosphorylated apo-APC/C. **e**, Local resolution map of APC/C$^{CDH1:Hsl1}$. **f**, Fourier Shell Correlation (FSC) plots of the main maps used to generate molecular models.

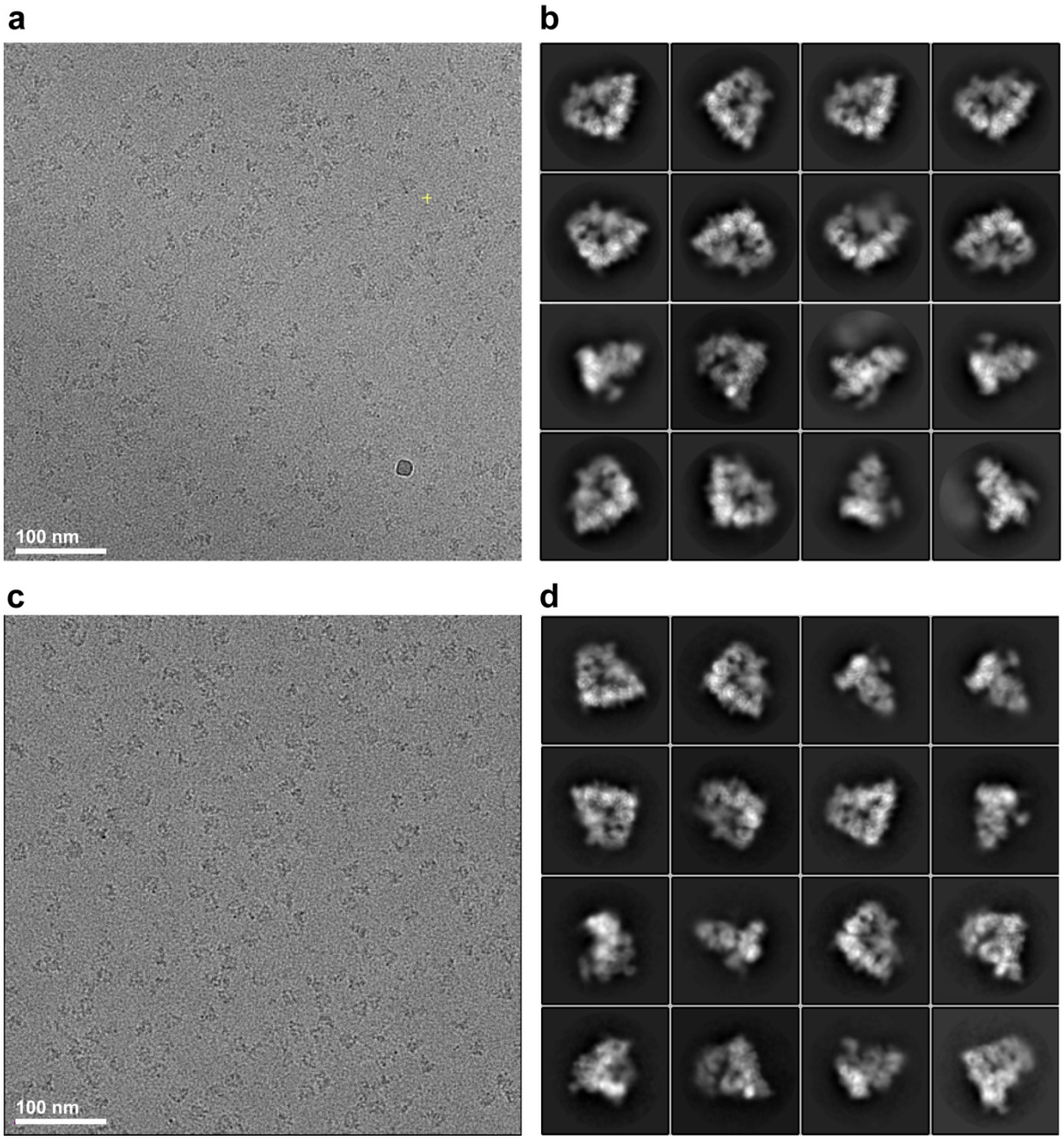

Supplementary Figure 3. Cryo-EM images and 2D class averages of apo-APC/C complexes. a, Representative cryo-EM image of unphosphorylated apo-APC/C. **b**, Gallery of 2D-class averages of unphosphorylated apo-APC/C. **c,** Representative cryo-EM image of phosphorylated apo-APC/C. **d**, Gallery of 2D-class averages of phosphorylated apo-APC/C.

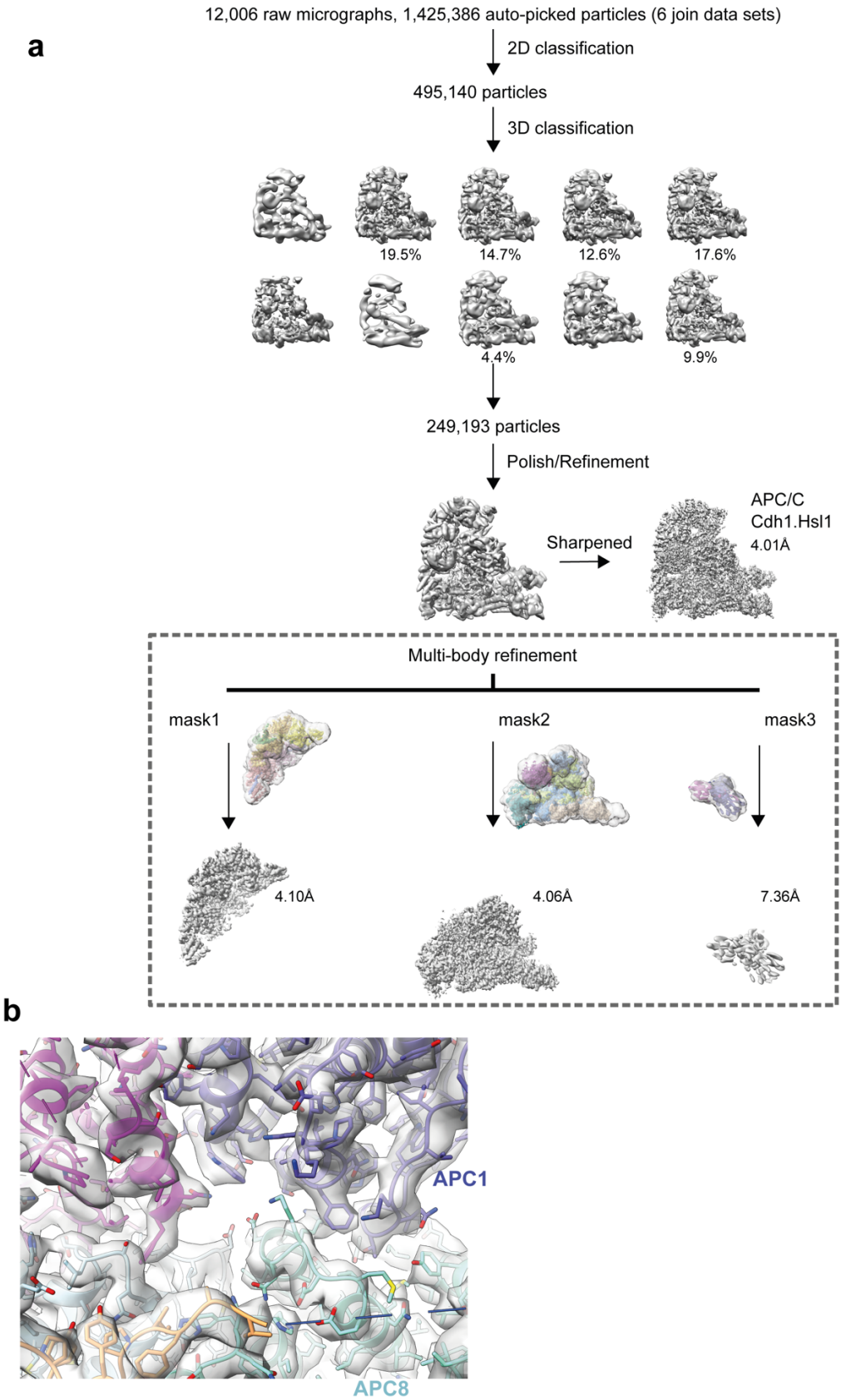

Supplementary Figure 4. Data processing pipeline for APC/C$^{CDH1:Hsl1}$ complex cryo-EM reconstructions. a, Cryo-EM data processing workflow summary for the APC/C$^{CDH1:Hsl1}$ complex as described in the Methods section. **b**, Example of cryo-EM map with fitted coordinates.

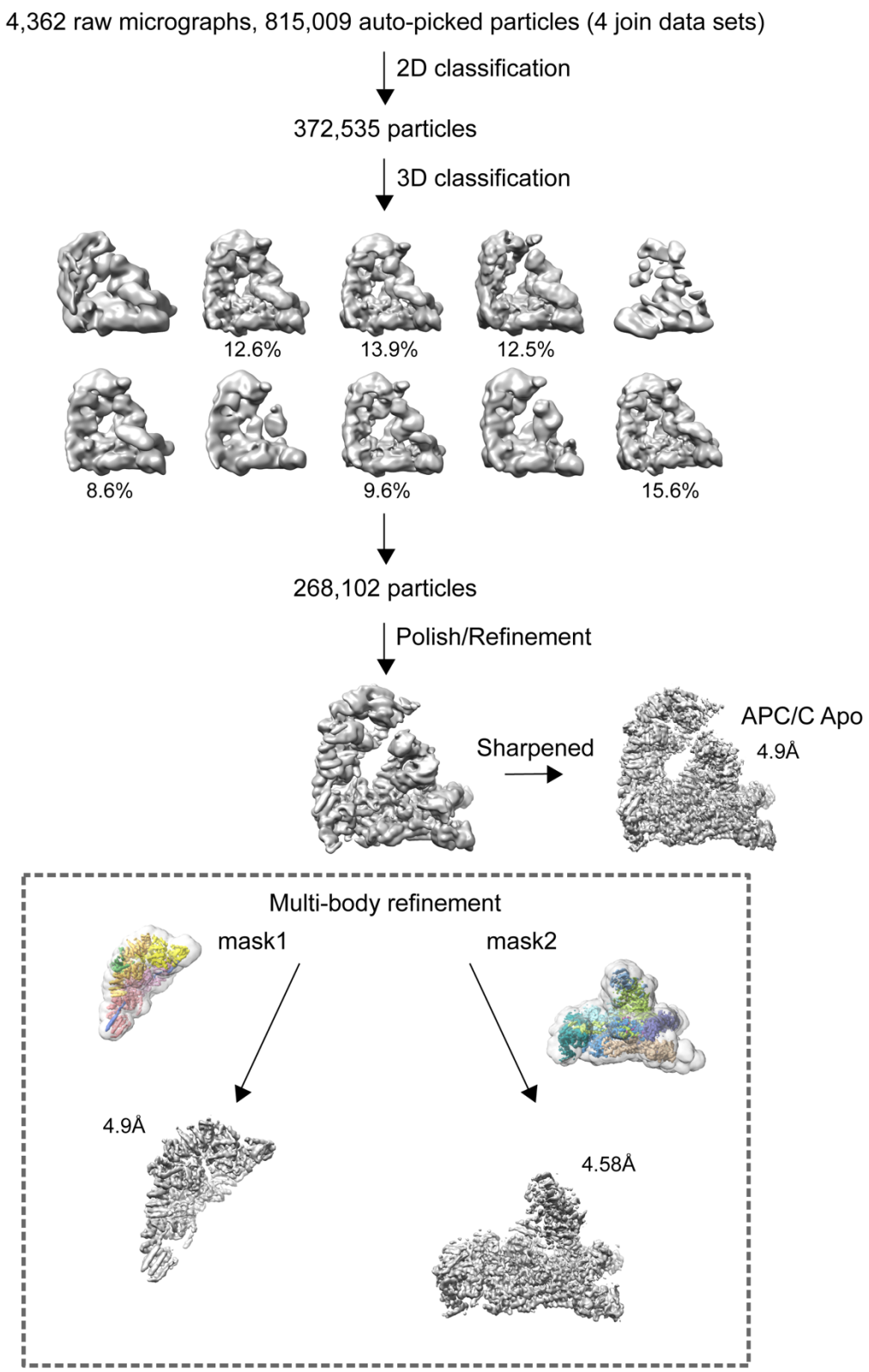

Supplementary Figure 5. Data processing pipeline for unphosphorylated apo-APC/C cryo-EM reconstructions. Cryo-EM data processing workflow summary for unphosphorylated apo-APC/C as described in the Methods section.

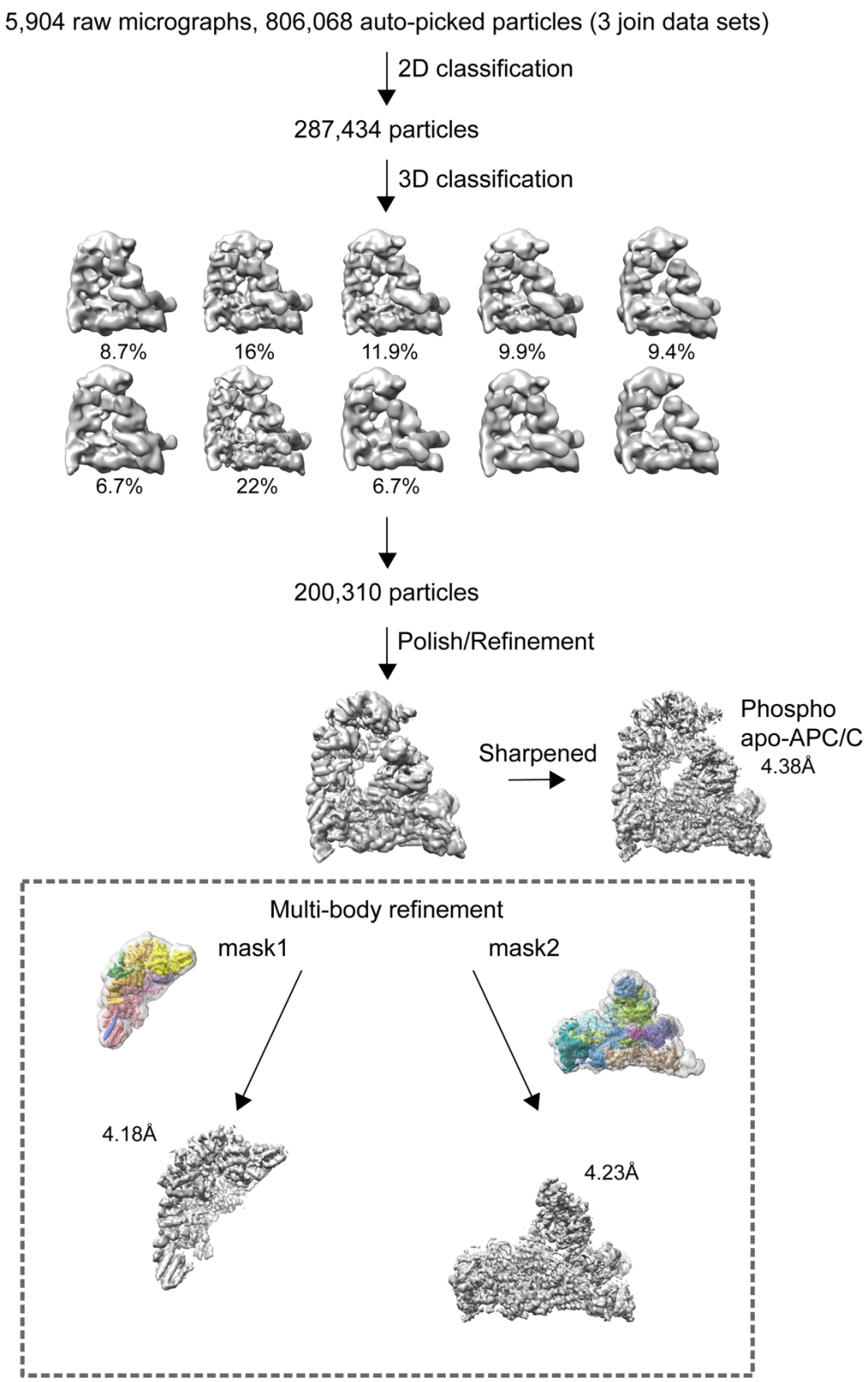

Supplementary Figure 6. Data processing pipeline for phosphorylated apo-APC/C cryo-EM reconstructions. Cryo-EM data processing workflow summary for phosphorylated apo-APC/C as described in the Methods section.

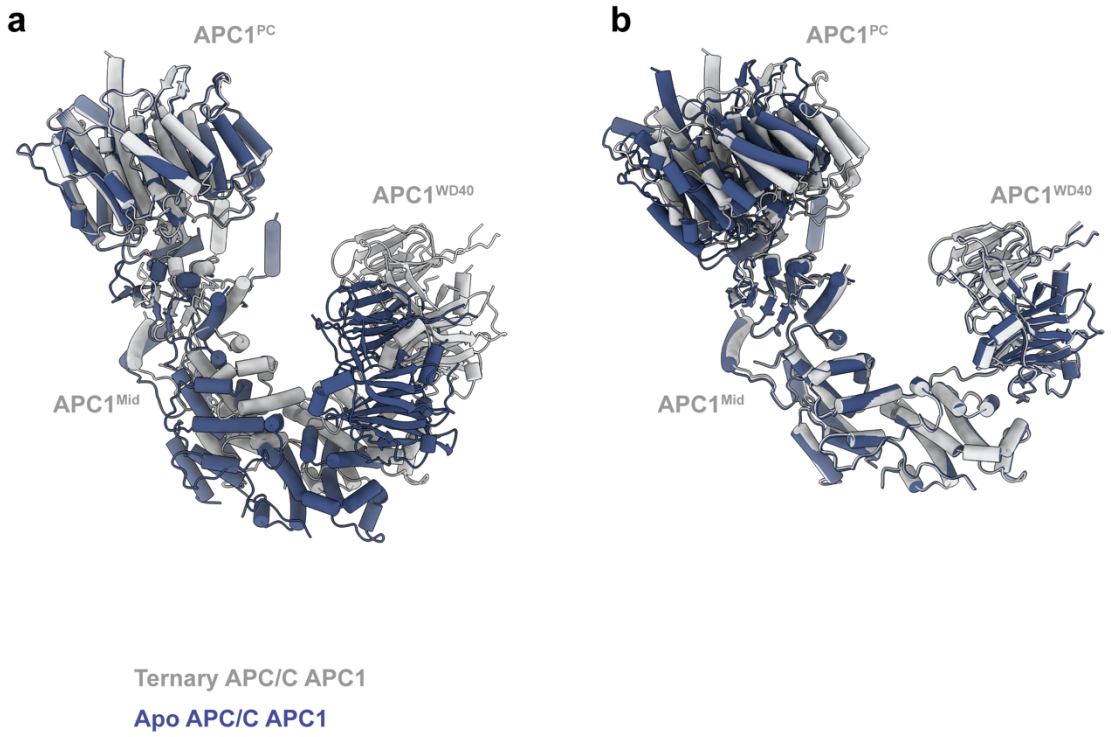

Supplementary Figure 7. Conformational change of APC1 on conversion from apo-APC/C to APC/C$^{CDH1:Hsl1}$. a, Superimposed on APC1^{PC}. **b**, Superimposed on the combined APC1^{Mid}-APC1^{WD40} domains. On conversion, there is a small tilt of APC1^{PC} relative to the combined APC1^{Mid}-APC1^{WD40} domains that form a rigid unit.

Supplementary Tables

Supplementary Table 1. CDK Phosphorylation site of *S. cerevisiae* APC/C

Supplementary Table 2. Cryo-EM data collection, refinement and validation statistics

Supplementary Table 3. Ordered and disordered regions of APC/C subunits

Supplementary Table 1. Summary of CDK phosphorylation sites of *in vitro* phosphorylated apo-APC/C identified by mass spectrometry

Protein	Phospho-sites									
APC1	S131	S133	T232	S234	S235	T236	S247	S250	S254	**S261**
	S267	**T268**	**S269**	S274	S285	S292	T295	S303	S305	**S308**
	S310	T312	T323	S329	S335	S336	T339	T341	S343	T346*
	S349	T363	T365	S444*	T499**	S500	S528	Y672	S678	S680
	T682	S691	T692	S702	S822	S838	S870	S872	S879	**S884**
	S897	T992	S1174	**S1192**	S1193	Y1206	S1208	**S1209**	S1418	S1433
	S1436	T1439	T1442	S1443	T1447*	S1451	T1459	**S1462**	**S1469**	S1560
	S1588	T1589*	S1647	S1669	T1681	S1683	S1688	T1695	T1701	T1709
	S1728	S1742								
APC3	T11	S13	S18	S134	S224	**S225**	S228	T229	S230	S232
	S238	S241	S244	T246	T260	**S265**	**S267***	S270	T271	S272
	S274	S275	S278	S285	T292	S293	T296	T304*	S312	S316
	S323	**S328***	S330	T335	S337	S338	**T350**	**T351***	S354	T394
	T397	S403	S404	T405	T409	T410	S423	T567	S585	S586
	T711	T719	T734							
APC2	**T81**	S82	S87	T268	T269	T270	T426	**S434***	T562	S572
	S706	S708	T735	S737	S742	T752	S760	S768	T777	S781
	S802	S842								
APC4	Y8	S143	S446	S459	S553	S554	S563	S578	S588	Y590
	S592	T596	Y598	Y603	T611	S635	S640	S642		
APC5	S68	S209	T262	S321	S341	S361	T366	S484	T497	S507
	S673									
APC8	S5	S25	T52	**S54**	**S59****	T94	**S135**	T141	T142	S159
	S167	S183	S185	S188	T337	S339	S370	S416	T531	S537
APC15	S9	**S51**	S71	S87	S101	T127	Y129	S136	T184	T189
	S193	S198	S222	Y223	T268	S269	**S273**	**S293**	S300	Y324
	S325	T329	S330	Y331	**T335***	T346	T351	**S352**		

Protein	Phospho-sites									
APC6	**S44***	**S46**	S50	S54	**T55**	S59*	S63	S66	T70	S73
	T76	T90	T92	**S95***	Y97	S99	S103*	T115*	S120	S123
	S127	S129	T131	S143	S145	S148	S152	T153	S156	T157
	S170	T209	T211	T212	T214	T215	T216	T217	T218	T220
	S225	S228	S305	S326	T331	T332	T336	S338	S344	S360
	S438	T447	**S449**	S468	T475	S734	Y736	S742	S743	T757
	S763	S770	S774	**S777**	S782	**S788**	**S789**	T791	**Y792**	
APC9	S17	T23**	T35	T36**	T43	S50	T54	T62	Y67	T81
	S83	S94*	S109	S159	T183	S185	S205	S210	S248	**S258**
	S262	S263								
APC10	S30	T85	T111	S223	T230	T236				
APC13	T79	S80	S121	T140	T142	S144	T151	S169		
APC11	S10	S15	S22	T84*	T145	T156				
APC12	T8	**S12**	T17	T37	T57	S58	S79	S96	S100	T101
	S103	T105	T109	**S110**						

The phosphorylation sites in **red** are present in both complexes: phosphorylated apo-APC/C and the control unphosphorylated apo-APC/C. The sequence coverage is ≥77% for all the subunits.
* Consensus CDK site (S/T)P
** Consensus CDK site (S/T)Px(K/R)

Supplementary Table 2. Cryo-EM data collection, refinement and validation statistics.

	Apo-APC/C (EMD-15199) (PDB 8A5Y)	Phosphorylated apo-**APC/C** (EMD-15201) (PDB 8A61)	**APC/C$^{CDH1:Hsl1}$** (EMD-15123) (PDB 8A3T)
Data collection			
EM	FEI Titan Krios	FEI Titan Krios	FEI Titan Krios
Detector	FEI Falcon III	FEI Falcon III	FEI Falcon III
Magnification	59,000	59,000	59,000
Voltage (keV)	300	300	300
Electron exposure (e-/Å^2)	59	59	59
Defocus range (μm)	2.6-3.9	2.6-3.9	2.6-3.9
Pixel size (Å)	1.38	1.38	1.38
Reconstruction			
Software	RELION 3.1	RELION 3.1	RELION 3.1
Symmetry imposed	C1	C1	C1
Initial particle images (N)	815,009	806,068	1,425,386
Final particle images (N)	268,102	200,310	249,193
Accuracy of rotations (°)	1.76	1.79	1.16
Accuracy of translations (°)	1.01	0.93	0.62
Map resolution (Å)	4.9	4.4	4.0
FSC threshold	0.143	0.143	0.143
Refinement			
Software	Phenix		
Resolution limit (Å)	4.9	4.4	4.0
RMSD bond length (Å)	0.004	0.003	0.004
RMSD bond angle (°)	0.878	0.641	0.754
Model to map fit			
CC_mask	0.756	0.793	0.752
CC_volume	0.748	0.785	0.750

Validation			
All-atom clash score	18.46	15.14	18.84
Ramachandran plot			
Preferred (%)	95.76	95.74	95.93
Allowed (%)	3.94	4.02	3.90
Outliers (%)	0.34	0.24	0.17